Deformations Associated With Relaxation of Residual Stresses in a Sample of Barre Granite From Vermont

GEOLOGICAL SURVEY PROFESSIONAL PAPER 875

Deformations Associated with Relaxation of Residual Stresses in a Sample of Barre Granite From Vermont

By T. C. NICHOLS, JR.

GEOLOGICAL SURVEY PROFESSIONAL PAPER 875

A study of measurable-mobilized strains that occur when a granitic rock sample, containing stored elastic deformational energy, is physically dissected in a systematic manner

UNITED STATES GOVERNMENT PRINTING OFFICE, WASHINGTON : 1975

UNITED STATES DEPARTMENT OF THE INTERIOR

ROGERS C. B. MORTON, *Secretary*

GEOLOGICAL SURVEY

V. E. McKelvey, *Director*

Library of Congress Cataloging in Publication Data
Nichols, T. C.
Deformations associated with relaxation of residual stresses in a sample of Barre Granite from Vermont.
(Geological Survey Professional Paper 875)
Based on the author's thesis study (M.S.), Texas A&M University.
Bibliography: p.
Supt. of Docs. no.: I 19.16:875
1. Rock deformation. 2. Granite—Vermont.
I. Title. II. Series: United States Geological Survey Professional Paper 875.
QE604.N52 522'.3 74-26896

For sale by the Superintendent of Documents, U.S. Government Printing Office
Washington, D.C. 20402 – Price $1.25 (paper cover)
Stock Number 024-001-02601

CONTENTS

ILLUSTRATIONS

TABLES

GLOSSARY OF UNCOMMON TERMS USED IN TEXT

Definitions used here are consistent with those of quoted authors or of others considered to be experts in the field.

Locking domain: A volume and shape in rock that can contain in equilibrium a particular system of internally balanced forces (Varnes and Lee, 1972).

Overcore: To make a cut with a core barrel around an instrumented volume of rock, separating that volume from the remaining rock mass.

Prestrain: Strain that results from prestress. The term alludes to locked-in, potentially recoverable strains that reflect rock distortions related to the history of internal or external loads.

Prestress: The term used in this text is synonymous with residual stress. The term alludes to that part of the previously applied internal or external forces which is stored as residual stress.

Residual strain: Locked-in, potentially recoverable elastic distortions, satisfying internal equilibrium conditions with no external loads or temperature gradients (Friedman, 1972).

Residual stress: A stress system satisfying internal equilibrium, with no external loads or temperature gradients (McClintock and Argon, 1966).

Strain relief or stress relief: The mobilization of stored elastic energy (stress or strain) by creating physical changes within an existing force field.

DEFORMATIONS ASSOCIATED WITH RELAXATION OF RESIDUAL STRESSES IN A SAMPLE OF BARRE GRANITE FROM VERMONT

By T. C. NICHOLS, JR.

ABSTRACT

A cube of Barre Granite (approximately 22 cm on a side), free of boundary loads, was sequentially and concentrically drilled out with 5.1-, 10.1-, and 15.0-cm core bits on the top and bottom sides and with a 10.1-cm core bit on a third side. The top and bottom sides are parallel to the grain or lift plane, which is horizontal in the quarry, and the third side is parallel to the rift plane, which is vertical and strikes N. 30° E. Strains resulting from overcoring were recorded on these sides with thirty-six 45°-rosette resistance strain gages.

The strain changes observed upon coring seem to have been derived from a complexly changing internal residual stress field. Initially, as the top surface was overcored, the resulting strain changes were mostly compressional; that is, the block contracted. Strain changes became more extensional as the bottom of the block was overcored. Finally, there were large net strain changes that were radially compressional and tangentially extensional, relative to each set of concentric overcores.

The largest strain changes were observed adjacent to freshly cut surfaces, yet significant changes were monitored over the entire surface of the block after each overcoring. Cumulative strain changes monitored on opposing gages symmetrically located across a freshly cut surface were, much of the time, similar in sense, magnitude, and direction.

The residual stress field is related to the changing geometry of the body, the induced free surfaces, and seemingly to the degree of homogeneity, orientations, and magnitudes of the stresses when they were frozen in. Cumulative strain changes at individual gage locations were large — as much as 330×10^{-6} (extension) and -275×10^{-6} (compression).

The deformation generally appears to be elastic. At certain gages, however, there were occasional large anomalous strain changes that are interpreted to result from permanent deformations, such as intergranular movements or intragranular gliding. These mechanisms may also be partly responsible for a pronounced creep event that was observed after the top 15.0-cm coring was completed; the whole block, which had initially contracted, expanded for 48 hours after the coring event, until the net strain change was nearly zero.

The extensional deformations typically occurring across a pilot borehole as a result of stress-relief overcoring techniques can be caused by at least two possible stress conditions an externally applied compressional stress field or the mobilized tensile component of the internal or residual stress field. When externally applied compressive forces are cut by overcoring, the innner and outer walls of the newly created annulus will expand. An internally balanced stress field may be partially relieved upon cutting of the outer cylindrical surface of the newly created annulus. If the tensile energy is relieved locally, then compressive strains are mobilized, causing the annulus to become thinner. The interior wall thus expands, and the exterior wall contracts. A deformation-measuring device placed in the interior hole measures extension of the interior wall in both stress conditions considered.

INTRODUCTION

With any deformation of a natural rock mass, whether manmade or natural, there is an accompanying disturbance of the preexisting quasistatic elastic stress field. The stresses, whether residual, gravitational, or present-day tectonic, are at least momentarily unbalanced, and energy is expended in some type of work or heat transfer. A better understanding of how released residual-elastic-strain energy is expressed at free boundaries is needed. Systematic quantitative knowledge of this phenomenon would be of great practical value for the design of mines, quarries, and engineering structures. Also, this knowledge may well be of value to earthquake prediction. I believe that the source of a significant quantity of the total energy released has been residual strain (stress). If the release of these stresses can be predicted quantitatively in terms of a stress and (or) strain tensor, the information will be valuable in design and construction practices.

In the present research, a systematic investigation of residual-strain relief was conducted to determine the magnitudes and distribution of the resulting strain changes as the geometry of a block of rock was modified and to discover the relation of these strains to fabric elements.

"Prestress," "residual stress," "prestrain," "residual strain," and other uncommon terms used in this text are defined in the glossary.

This report is based on a thesis study conducted at Texas A & M University in partial fulfillment of the requirements for the Master of Science degree.

ACKNOWLEDGMENTS

I am pleased to acknowledge the active support, criticism, thoughtful comments, and many ideas provided by Melvin Friedman, John W. Handin, David W. Stearns, David J. Varnes, Fitzhugh T. Lee, and John F. Abel, Jr.

Thomas A. Bur, U.S. Bureau of Mines, supplied the block of Barre Granite upon which the experiment was

performed. The U.S. Geological Survey and the Advanced Research Projects Agency provided much of the instrumentation and apparatus necessary to perform the experiment.

PREVIOUS WORK

RECOGNITION OF RESIDUAL STRESS

The existence of residual stress in rocks and rock masses has been recognized for a long time — at least 180 years (Varnes, 1969). Much thought has been given recently to this subject (Lowry, 1959; Pincus, 1964; Friedman, 1967, 1971, 1972; Denkhaus, 1967; Voight, 1967; Emery, 1968; Nichols and others, 1969; Price, 1969; Hoskins and Daniels, 1970). Several of these authors have made measurements of residual strains in laboratory experiments. Price (1969, p. 7) observed siltstone specimens that expanded in creep under uniaxial compressive loads of 640 bars and greater, and he attributed this expansion to the release of residual stresses. Friedman (1967) used X-ray techniques to determine the existence of residual elastic strains within quartzose rocks. Also, Friedman and Logan (1970) related similarly determined data to the orientations of fractures induced in quartzose rock specimens under controlled boundary loads. Friedman (1971, 1972) has summarized information about residual strains, primarily from his X-ray studies.

INVESTIGATIONS TO DETERMINE THE NATURE OF RESIDUAL STRESS

Very few investigations have been undertaken to determine the extent of the relief of residual stresses within rock masses and the manner in which the released energy is expressed at free rock boundaries.

Emery (1964) used photoelastic transducers to demonstrate the existence of elastic strain energy in sandstones, foliated quartzites, granites, and pebble conglomerates. He concluded that these rocks contain substantial amounts of potential elastic strain energy that in some cases is recoverable and that has pronounced measurable anisotropy.

Pincus (1964) also used photoelastic transducers, and he was able to demonstrate that 5.4-cm(NX)-diameter rock disks, relieved by small-diameter (0.4-cm) holes, showed relief patterns around the holes.

Sharp (1969) made residual-stress determinations on core samples taken from the Red Mountain mid-Tertiary intrusive complex, west of Denver, Colo. The determined secondary principal stresses were attributed to stored energy related to the forcible emplacement of a mid-Tertiary stock. Also, Sharp alluded to the relief of strain as a possible cause of failure for future mine shafts in the area.

Varnes (1969) designed and built a physical model consisting of individual units representing grains in a rock. The model behavior simulates that of stress relief within a rock. The grain units capable of interacting viscously and elastically with elastic and frictional restraints. Varnes stated that experiments are in progress to detect effects of size and geometry of the model.

E. G. Bombolakis (in Friedman and Logan, 1970, p. 387) attempted to determine the size effects on relieving residual stresses by overcoring. Starting with 12.5-cm cores of granite near Chelmsford, he successively overcored 45°-rosette resistance strain gages with 7.5-, 5.4-, and 3.8-cm core bits, and after each overcoring he measured still further strain relief.

Hoskins and Daniels (1970) determined directions and relative magnitudes of residual strains in six different specimens by undercoring with different sized core bits. J. F. Abel, Jr., and T. C. Nichols, Jr., performed similar experiments in U.S. Geological Survey laboratories on Precambrian metasedimentary and granitic rocks from Colorado and on Paleozoic granite from North Carolina.

Friedman (1971) conducted experiments in which he measured residual strains in the grains of naturally deformed sandstones. Using X-ray techniques, Friedman compared the "before" and "after" state of residual strain in individual sandstone grains that were relieved by etching with hydrochloric and hydrofluoric acids. Similarly, he compared the "before" and "after" state of residual strain in individual sand grains of laboratory-compacted and welded specimens, freed merely by etching with water.

Gallagher (1971) concluded from photoelastic model studies that residual elastic strains detected in sandstones by X-ray method are average values that include the strains within the grains and the cementing matrix over the volume scanned.

THE BARRE GRANITE

Barre Granite was chosen for this experiment because much work had already been done on its mineralogy and on the nature of its elastic anisotropy.

White (1946) recognized that much nonuniform energy is relieved in quarry operations at Barre, Vt.; Hooker and Johnson (1969) measured the in situ stress field in the Smith granite quarry and at nearby outcrops close to Barre, and they made laboratory measurements on cores from which values of the anisotropic elastic moduli were calculated.

Douglass and Voight (1969) found microfractures and fluid inclusions (healed microfractures) to be strongly oriented parallel to the rift plane, which is vertical and strikes about N. 80° E. They found a smaller concentration of microfractures in the grain direction parallel to the horizontal lift plane, but where the quartz optic axes are strongly oriented parallel to the rift plane, they related these features to the laboratory-determined compliance ellipsoid.

Willard and McWilliams (1969) found a similar strong concentration of fractures parallel to the plane of easiest tensile fracture, which is most likely the rift plane.

Bur, Hjelmstad, and Thill (1969) measured velocities and relative sonic amplitudes within the Barre Granite that show well-developed orthotropic symmetry. The plane containing the axes of highest and intermediate velocity and relative amplitude coincides with the rift plane, wheras the plane containing the axes of highest and intermediate attenuation coincides with the hardway plane (M. Friedman, oral commun., 1971).

Melvin Friedman (oral commun., 1971) used X-ray-diffraction techniques to determine the state of prestress (residual stress). The chip of granite used for that determination was taken from the block used in the experiment for the present report.

Nur and Simmons (1969) and Nur (1971) showed that acoustic birefringence is induced by stress in the Barre Granite and that the velocity anisotropy is dependent on both crack distribution and orientation of applied load.

The mineral composition of the Barre Granite, as determined by Chayes (1952), is as follows:

Mineral	*Percent*
Quartz	25
Potash feldspar	20
Plagioclase feldspar	35
Biotite	9
Muscovite	9
Accessories	1

The block used here has a similar modal composition and has an average grain size of about 2.0 mm.

EXPERIMENTAL PROCEDURE

A block of Barre Granite from the Wetmore and Morris quarry near Barre, Vt., was supplied for this experiment by T. R. Bur, Geophysicist, Twin Cities Mining Research Center, U.S. Bureau of Mines, Minneapolis, Minn. The block, nearly cubic and 22 cm on a side, was taken from a larger master block excavated at the quarry level 67 m below the ground surface, and it is oriented so that the sides are parallel to the rift, hardway, and grain direction (fig. 1). The top and bottom of the block are parallel to the grain or lift direction, sides 1 and 3 are parallel to the hardway plane, and sides 2 and 4 are parallel to the rift plane. The rift plane in this quarry strikes N. 30° E. (T. R. Bur, oral commun., 1971), and the grain is approximately horizontal.

The experiment was conducted in three phases, as follows:

Phase I. The determination of principal strain changes that occur on the surface of the block as a result of the systematic creation of new surfaces by core drilling.

Phase II. The observation of surface fabric changes that result from the creation of new surfaces.

Phase III. A cursory petrofabric examination to corroborate known anisotropy of fabric elements and to determine possible changes in fabric caused by the creation of new surfaces.

PHASE I

INSTRUMENTATION

Initially the block was polished on three surfaces: the top, bottom, and side 2 (fig. 1). Then 45°-rosette resistance strain gages were mounted on the polished surfaces and numbered as in the configuration shown in figure 1*B*. The rosettes marked F_1, F_2, and Q are those placed on individual feldspar and quartz grains. The grid elements of these three rosettes have a gage length of 0.76 mm. The rest of the rosettes have grid elements with gage lengths of 3.18 mm, and they cover several crystals or grains at each location. The gage circuit consisted of a half bridge with the sensing gage in the active arm and a compensating gage, mounted on a wafer of Barre Granite, in the compensating arm. Strain readings were made with a Budd SR4 Strain Indicator. The temperature during readings never varied more than 0.3°C and, during the experiment, ranged from 21.0° to 23.0°C. Changes of strain were calculated from readings that were taken within 0.3°C of each other.

SPURIOUS SIGNALS ASSOCIATED WITH THE EXPERIMENTAL TECHNIQUE

Before the strain-relief experiment was started, three initial checks were made to determine the approximate deviations of strain readings associated with the experimental procedures themselves.

1. Because the block was to be stress relieved by creating new surfaces with a diamond-drill bit, it was desirable to determine the effect of drilling water. Therefore, one of the faces was flooded and allowed to dry in a 12-hour period. By randomly comparing before and after readings of individual gages in three rosettes (a total of seven gages), it was found that the average deviation was only 7×10^{-6}.

2. Before and after each drilling operation, wire leads had to be unsoldered and soldered. Before and after readings on four gages unsoldered and resoldered had an average deviation of only 3×10^{-6}.

3. Each of these checks included changes caused by switching the circuits through a low-resistance wafer switch and changes due to drift of the strain indicator. The combined switch and strain indicator deviation was 2×10^{-6} per degree.

Thus the probable "accidental error" after any single drilling operation is probably no greater than 10×10^{-6} if readings are taken with 0.3°C of each other.

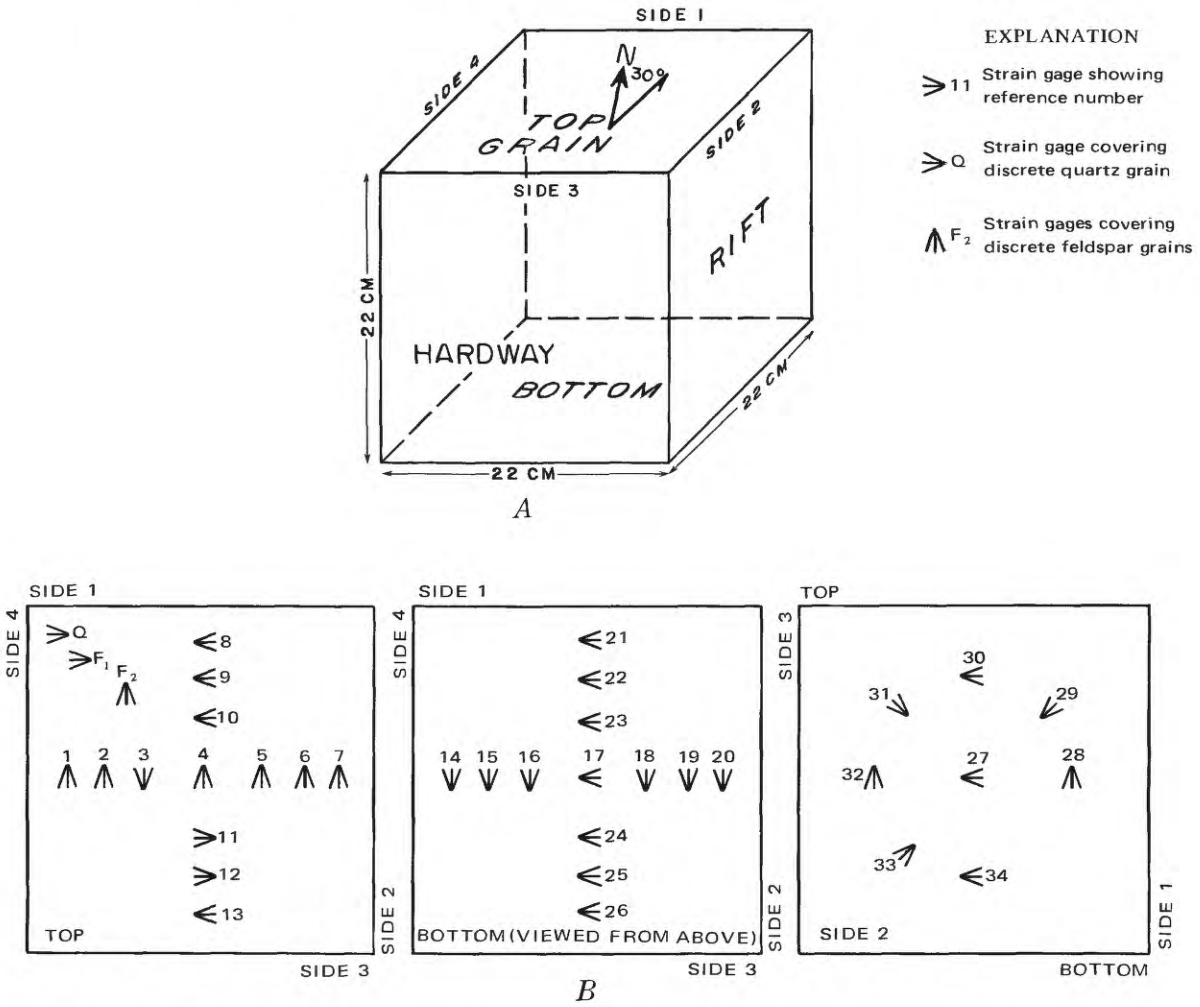

FIGURE 1. — Block of Barre Granite used in this experiment. *A*, Block showing rift, grain, and hardway planes. *B*, Top, bottom, and side-2 faces of block showing positions of the 45°-strain rosettes.

SUCCESSION OF CORING AND COLLECTION OF DATA

After the initial checks were made, the strain gages were read once a day for 3 days, and during this time the block was stable within $\pm 5 \times 10^{-6}$. After the 5.1- and 10.1-cm cuts, the strain changes ceased after the first 24 hours. After the 15.0-cm coring there was a creep event at all gages over 48 hours.

When the block had stabilized, the cores created by drilling were broken out (fig. 2), and slight further strain relief occurred. The block was then turned over and drilled successively on the bottom face in the same manner as before (fig. 3). The depth of the cuts, however, was only 9.5 cm, and the cuts did not penetrate to the hole already drilled from the top side. Thus, each core was still attached to a small thickness of rock. Strain changes recorded after each of the bottom cuts largely ceased within 12 hours. There were, however, four grid elements in separate rosettes that showed small creep after the 5.1-cm cut. These circuits were checked for bad solder joints, worn leads, or bad switch connections, but none were found.

FIGURE 2. — Top of block after annuli have been broken out. Core is 10.1 cm in diameter.

FIGURE 3. — Bottom of block after successively coring with 5.1-, 10.1- and 15.0-cm core bits.

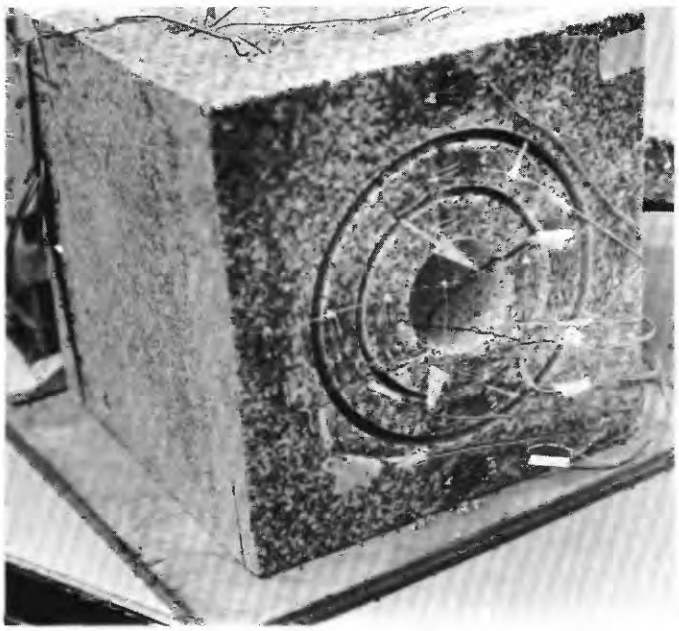

FIGURE 4. — Bottom of block showing fractured interior annulus (arrow).

An attempt was made to break the cores free from the rock, as had been done at the top. However, the interior annulus was chipped at the lip (fig. 4), leaving two small rock fragments free of the annulus with the strain rosette still intact. It was decided then to leave the other annulus intact until the experiment was finished.

This phase of the experiment was completed when the block was again rotated and side 2 (fig. 5) was cut with a 10.1-cm bit to a depth of nearly 13 cm, thus nearly freeing the core on the bottom. The strain changes that accurred after this cut also ceased within 12 hours.

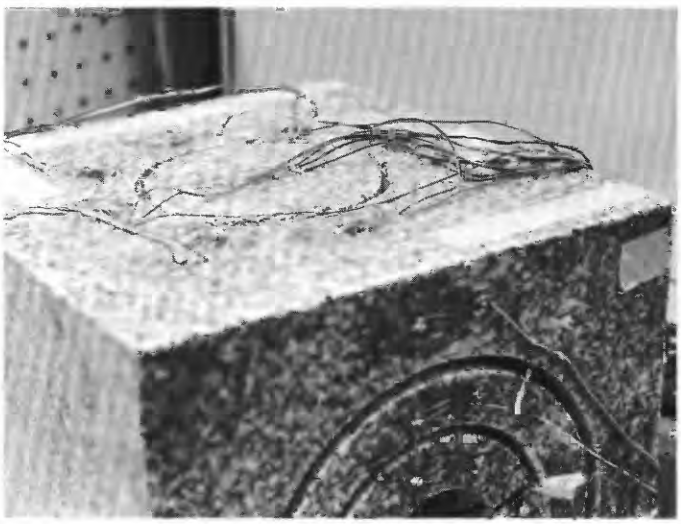

FIGURE 5. — Side 2 after coring with 10.1-cm core bit.

PHASE II

OBSERVATION OF SURFACE FABRIC

Changes in the rock fabric that occurred as a result of the coring were looked for — specifically, the development of microfractures on the top surface of the block.

In order to emphasize the fabric elements, especially microfractures and grain boundaries, several staining techniques were attempted. The most successful was a penetrant organic dye that emphasized both the microfractures and the grain boundaries (Gardner and Pincus, 1968). The part of the top surface stained for observation covered approximately one-half of the northeast quadrant and extended from the outer edge of the block to within 5 cm of the center. For the purpose of comparing fabric elements after strain relief, large-scale photographs were made at identical locations before and after the block was drilled (fig. 6). The location seen in figures 6*A* and 6*B* is about midway between gages 6 and 9, and the location seen in figures 6*C* and 6*D* is about midway between gages 7 and 8.

PHASE III

PETROFABRIC EXAMINATION

Extensive petrofabric analysis of the Barre Granite has been done by Douglass and Voight (1969) and Willard and McWilliams (1969). Nonetheless, two sets of three mutually orthogonal thin sections from the block used in this experiment were examined to corroborate the anisotropy of petrofabric elements. Also, these sections were examined to discover changes in the fabric produced by overcoring. The thin-section locations were chosen in an area of (1) high strain relief directly under gage 6 (fig. 1), and (2) moderate strain relief 5 cm below gage 4 (fig. 1).

EXPERIMENTAL RESULTS

PHASE I

PRESENTATION OF STRAIN DATA

Strain data were recorded at all locations after each coring of the block. Changes of strain were used to calculate the maximum and minimum (secondary) principal strain changes by the rectangular-rosette method (Frocht, 1941, p. 37). The maximum principal strain changes ($\Delta\epsilon_1$) were regarded as most extensional, and the least principal strain changes ($\Delta\epsilon_2$) as least extensional; extensional strain was taken as positive and compressional strain as negative. The principal strain changes so calculated are changes in response to the cutting of new surfaces. The residual strains are those, with reference to an original undisturbed state of zero strain, that occurred when the stored energy was locked in; therefore, they are opposite in sign to the relieved strains measured experimentally. It is important to note that data on strain changes are mostly those determined from either of two zero readings; namely, (1) the initial reading prior to any drilling of the block, and (2) the stable reading after completely coring the top but prior to any coring on the bottom. Strain changes ($\Delta\epsilon$) relating to these readings will be denoted $\Delta_0\epsilon$ and $\Delta_B\epsilon$, respectively. Any other zero points will be specified in the text.

The strain differences $\Delta\epsilon$ at all gages shown in tables 1 and 2 were calculated from stable readings 24 hours after each coring. The stable 48-hour reading after the 15.1-cm coring on the top surface was made because the 24-hour reading was not stable. Arms *a*, *b*, and *c* designate the individual gages on each rosette, arm *a* being the most clockwise and arm *c* the most counterclockwise. Individual gage orientations are shown in figure 1.

TABLE 1. — *Strain differences, $\Delta_0\epsilon$ and $\Delta_B\epsilon$, at gages 1 through 34*

[The strain differences at all gages were calculated from stable readings 24 hours after each coring, except as noted. Arms *a*, *b*, and *c* designate individual gages on each rosette, arm *a* being the most clockwise and arm *c* the most counterclockwise. Individual gage orientations are shown in fig. 1. Leaders (- - - -) indicate no data available]

Gage No.	Arm	$\Delta_0\epsilon$ ($\times 10^{-6}$) based on stable zero reading prior to 5.1-cm coring on top face				$\Delta_B\epsilon$ ($\times 10^{-6}$) based on stable zero reading prior to 5.1-cm coring on bottom face			
		After 5.1-cm coring on top face	After 10.1-cm coring on top face	After 15.0-cm coring on top face	After 15.0-cm coring on top face (48 hrs[1])	After 5.1-cm coring on bottom face	After 10.1-cm coring on bottom face	After 15.0-cm coring on bottom face	After 10.1-cm coring on side face
1	*a*	−10	−13	3	14	- - - -	- - - -	- - - -	- - - -
	b	−3	−16	39	57	- - - -	- - - -	- - - -	- - - -
	c	−1	−18	1	15	- - - -	- - - -	- - - -	- - - -
2	*a*	−5	−45	−63	−51	- - - -	- - - -	- - - -	- - - -
	b	7	54	84	91	- - - -	- - - -	- - - -	- - - -
	c	3	−116	−109	−94	- - - -	- - - -	- - - -	- - - -
3	*a*	−57	−102	−93	−58	- - - -	- - - -	- - - -	- - - -
	b	20	−40	−25	−9	- - - -	- - - -	- - - -	- - - -
	c	−6	−111	−98	−65	- - - -	- - - -	- - - -	- - - -
4	*a*	−76	−98	−82	−51	- - - -	- - - -	- - - -	- - - -
	b	−55	−60	−49	−23	- - - -	- - - -	- - - -	- - - -
	c	−52	−62	−55	−32	- - - -	- - - -	- - - -	- - - -
5	*a*	−51	−125	−132	−105	- - - -	- - - -	- - - -	- - - -
	b	2	−43	−36	−7	- - - -	- - - -	- - - -	- - - -
	c	−21	−183	−176	−154	- - - -	- - - -	- - - -	- - - -
6	*a*	−3	−51	−69	−54	- - - -	- - - -	- - - -	- - - -
	b	−17	−21	−19	11	- - - -	- - - -	- - - -	- - - -
	c	−12	−38	−141	−118	- - - -	- - - -	- - - -	- - - -
7	*a*	6	−3	−2	19	34	28	27	16
	b	−5	−7	20	40	19	9	27	6
	c	10	14	22	40	30	18	26	16
8	*a*	−27	−17	−21	22	34	39	- - - -	- - - -
	b	−15	−14	15	41	63	0	- - - -	- - - -
	c	12	45	48	139	28	16	- - - -	- - - -
9	*a*	−10	−17	−14	8	- - - -	- - - -	- - - -	- - - -
	b	−2	6	6	10	- - - -	- - - -	- - - -	- - - -
	c	−8	−23	−113	−98	- - - -	- - - -	- - - -	- - - -
10	*a*	−65	−84	−66	−53	- - - -	- - - -	- - - -	- - - -
	b	40	−12	1	11	- - - -	- - - -	- - - -	- - - -
	c	−11	−152	−134	−137	- - - -	- - - -	- - - -	- - - -
11	*a*	−58	−106	−94	−77	- - - -	- - - -	- - - -	- - - -
	b	19	−53	−43	−23	- - - -	- - - -	- - - -	- - - -
	c	−27	−73	−58	−42	- - - -	- - - -	- - - -	- - - -
12	*a*	−16	−174	−167	−142	- - - -	- - - -	- - - -	- - - -
	b	−14	30	44	72	- - - -	- - - -	- - - -	- - - -
	c	0	−23	−29	−11	- - - -	- - - -	- - - -	- - - -
13	*a*	−8	−16	−9	16	24	13	27	10

TABLE 1. — *Strain differences, $\Delta_{0\epsilon}$ and $\Delta_{B}\epsilon$, at gages 1 through 34* — Continued

Gage No.	Arm	$\Delta_{0\epsilon}$ ($\times 10^{-6}$) based on stable zero reading prior to 5.1-cm coring on top face: After 5.1-cm coring on top face	After 10.1-cm coring on top face	After 15.0-cm coring on top face	After 15.0-cm coring on top face (48 hrs[1])	$\Delta_{B}\epsilon$ ($\times 10^{-6}$) based on stable zero reading prior to 5.1-cm coring on bottom face: After 5.1-cm coring on bottom face	After 10.1-cm coring on bottom face	After 15.0-cm coring on bottom face	After 10.1-cm coring on side face
	b	−6	−6	24	47	26	16	26	13
	c	0	6	4	36	20	−17	26	7
14	*a*	−11	−29	4	17	9	15	6	25
	b	−18	−32	−10	0	−2	11	48	22
	c	−5	−20	−12	0	15	27	28	28
15	*a*	−19	−35	−9	0	4	−14	−28	41
	b	−16	−35	−6	1	5	39	−6	30
	c	−15	−31	−7	5	−4	10	−61	32
16	*a*	−18	−32	−7	1	−39	4	7	46
	b	−20	−47	−18	−1	41	17	20	0
	c	−21	−38	−8	−6	−10	−33	6	55
17	*a*	−13	−30	−12	−2	−22	−1	18	----
	b	−17	−28	−12	6	−28	6	29	----
	c	−17	−37	−3	10	−29	−1	32	----
18	*a*	−23	−43	−27	−11	−40	−52	3	32
	b	−24	−46	−25	−8	30	−26	9	32
	c	−25	−45	−20	−7	−5	2	−2	69
19	*a*	−25	−41	−18	−1	6	3	−67	32
	b	−25	−47	−20	−6	8	39	−36	29
	c	−24	−46	−25	−14	4	−32	−21	28
20	*a*	−19	−33	−14	0	11	10	22	24
	b	−22	−39	−15	−4	7	11	43	30
	c	−18	−39	−20	−11	20	16	−7	34
21	*a*	−9	−20	14	5	10	24	18	30
	b	−5	−12	22	14	25	40	85	35
	c	3	−5	20	13	28	32	26	30
22	*a*	−13	−16	37	62	11	8	−20	29
	b	−15	−33	−1	−16	7	−54	−15	33
	c	−7	−18	49	66	35	103	−8	65
23	*a*	−17	−33	−26	−21	−28	−4	7	8
	b	−14	−36	−22	−32	22	−22	11	13
	c	−20	−31	−1	6	2	−39	7	15
24	*a*	−13	−35	−3	3	4	−35	17	−30
	b	−16	−34	−7	−7	38	8	10	26
	c	−18	−41	−19	−13	−18	7	7	47
25	*a*	−14	−24	−2	8	12	17	−26	----
	b	−19	−37	−13	−4	19	45	−30	----
	c	−14	−30	−26	−11	4	−37	−52	----
26	*a*	−16	−28	−14	−5	5	13	33	27
	b	−8	−22	0	8	16	38	76	29
	c	−8	−20	−1	6	14	29	23	29
27	*a*	−23	−34	−15	−1	15	11	14	−1
	b	−17	−14	12	26	9	7	30	9
	c	−19	−28	−11	3	10	9	8	12
28	*a*	−13	−20	−2	9	9	9	2	2
	b	−6	−3	24	41	16	13	6	46
	c	−8	−8	9	25	11	2	2	20
29	*a*	----	----	----	----	----	----	----	−6
	b	----	----	----	----	----	----	----	−48
	c	----	----	----	----	----	----	----	−32
30	*a*	−2	−6	12	26	6	17	13	12
	b	−4	−9	12	22	13	33	14	42
	c	−13	−24	−6	4	8	10	15	24
31	*a*	----	----	----	----	----	----	----	29
	b	----	----	----	----	----	----	----	10
	c	----	----	----	----	----	----	----	26
32	*a*	−10	−19	2	12	14	18	0	17
	b	−22	−33	−7	7	6	4	8	28
	c	−17	−26	2	9	19	6	13	16
33	*a*	----	----	----	----	----	----	----	16
	b	----	----	----	----	----	----	----	4
	c	----	----	----	----	----	----	----	16
34	*a*	−33	−53	−37	−24	8	1	12	12
	b	−27	−41	−17	−5	12	17	31	25
	c	−26	−44	−38	−18	5	8	10	12

[1]The 48-hour reading was made because the 24-hour reading was not stable.

TABLE 2. — *Strain differences, $\Delta\epsilon$ and $\Delta_B\epsilon$, at gages F_1, F_2, and Q*

[The strain differences at all gages were calculated from stable readings 24 hours after each coring, except as noted. Arms *a*, *b*, and *c* designate individual gages on each rosette, arm *a* being the most clockwise and arm *c* the most counterclockwise. Individual gage orientations are shown in fig. 1. Leaders (- - - -) indicate no data available]

Gage No.	Arm	$\Delta\epsilon$ ($\times 10^{-6}$) based on a stable zero reading prior to the 10.1-cm coring on top face			$\Delta_B\epsilon$ ($\times 10^{-6}$) based on a stable zero reading prior to the 5.1-cm coring on bottom face		
		After the 10.1-cm coring on top face	After the 15.0-cm coring on top face	After the 15.0-cm coring on top face (48 hrs[1])	After the 5.1-cm coring on bottom face	(41 days)	After the 10.1-cm coring on bottom face
F_1	*a*	−25	−46	2	62	23	131
	b	−17	42	76	19	24	78
	c	−4	25	53	86	43	148
F_2	*a*	−51	−75	−49	- - - -	- - - -	- - - -
	b	−80	−149	−106	- - - -	- - - -	- - - -
	c	−55	−83	−34	- - - -	- - - -	- - - -
Q	*a*	−41	16	55	37	19	36
	b	−32	18	62	0	15	64
	c	−37	23	55	34	1	21

[1]The 48-hour reading was made because the 24-hour reading was not stable.

Figures 6-13 show vectors representing the computed principal strain changes at each gage location on the top, bottom, and side-2 surfaces after each coring operation. At locations where strains are not shown, the strain values were very small or the gages were destroyed by drilling. Also plotted in figures 6 and 7*D* are vector representations of the prestrain contained within quartz grains as determined by X-ray diffraction techniques from chips taken from the same block. Prestrain has an opposite sense to strain caused by overcoring.

Figures 6, 7, and 8 show the principal strain changes $\Delta_0\epsilon_1$ and $\Delta_0\epsilon_2$ that occur on the top, bottom, and side-2 surfaces after each of the 5.1-, 10.1-, and 15.0-cm corings of the top surface. Figures 9, 10, and 11 show strain changes on top, bottom, and side-2 surfaces after similar corings of the bottom surface and after the 10.1-cm coring of side 2.

Figures 11, 12, and 13 show the principal strain changes that occur at the individual feldspar- and quartz-grain rosettes. Figure 12 shows these changes after the 10.1- and 15.0-cm corings of the top surface, The initial readings for these changes were taken after the 5.1-cm coring. Figure 13 shows these changes after the 5.1- and 10.1-cm corings of the bottom surface.

The pertinent strain-change data are presented in the following succession:

1. $\Delta_0\epsilon$ on the top surface after the 5.1-cm coring on top (fig. 6). After the 5.1-cm coring, the only significant strain changes on the block occurred in the vicinity of the freshly cut surface (fig. 6). The minor principal strain changes, $\Delta_0\epsilon_2$, are all compressional and of large magnitudes (up to -120×10^{-6}), whereas $\Delta_0\epsilon_1$ are either extensional or compressional but very small in magnitude (less than 40×10^{-6}). The orientation of the $\Delta_0\epsilon_2$ and $\Delta_0\epsilon_1$ axes on the outside of the circular cut is nearly radial and tangential to the cut, respectively, whereas the similar axes at the center of the core (gage 4) do not seem to closely aline with those on the outside.
2. $\Delta_0\epsilon$ on the top, bottom, and side 2 after the 10.1-cm coring on top (fig 7). After the 10.1-cm coring on top, the cumulative strain changes $\Delta_0\epsilon$ on all surfaces are significant. The larger $\Delta_0\epsilon$, however, are on the top surface near the newly created 10.1-cm circular cut (fig. 7*B*). The $\Delta_0\epsilon_2$ are all compressional, with magnitudes as large as -250×10^{-6}; and the $\Delta_0\epsilon_1$ are either compressional or extensional, with magnitudes of as much as 60×10^{-6}. The larger $\Delta_0\epsilon_2$ and $\Delta_0\epsilon_1$ axes, both exterior and interior to the 10.1-cm diameter cut, tend to be radial and tangential, with noticeable rotation at gages 11 and 12. Within the zone just outside the cut, at gages 6 and 9, the $\Delta_0\epsilon_2$ are much less compressive than those at gages 2 and 12, and, conversely, at gages 5 and 10 on the newly formed annulus across the cut from 6 and 9, and $\Delta_0\epsilon_2$ are more compressive than at similar gages 3 and 11 diametrically opposite, across the cut from 2 and 12. The unequal strain behavior at these gages is even more clearly demonstrated in figure 7*A*, which shows the principal strain changes that occurred between the 5.1-cm and the 10.1-cm coring. The $\Delta_0\epsilon_2$ and $\Delta_0\epsilon_1$ on the center core changed only slightly (fig. 7*A*).

The $\Delta_0\epsilon$ on the bottom and side-2 surfaces (figs. 7*C*, 7*D*) are nearly all compressive and have magnitudes commonly as large as -65×10^{-6}.

On the bottom surface, the $\Delta_0\epsilon_2$ and $\Delta_0\epsilon_1$ axes aline very well with those of similar positions on the top surface.

The $\Delta_0\epsilon_2$ and $\Delta_0\epsilon_1$, nearly all compressive on the bottom surface, are larger toward the center, thus reflecting the radial disturbance on top.

The $\Delta_0\epsilon$ on side 2, all compressive, are small near the top of the block but become larger toward the bot-

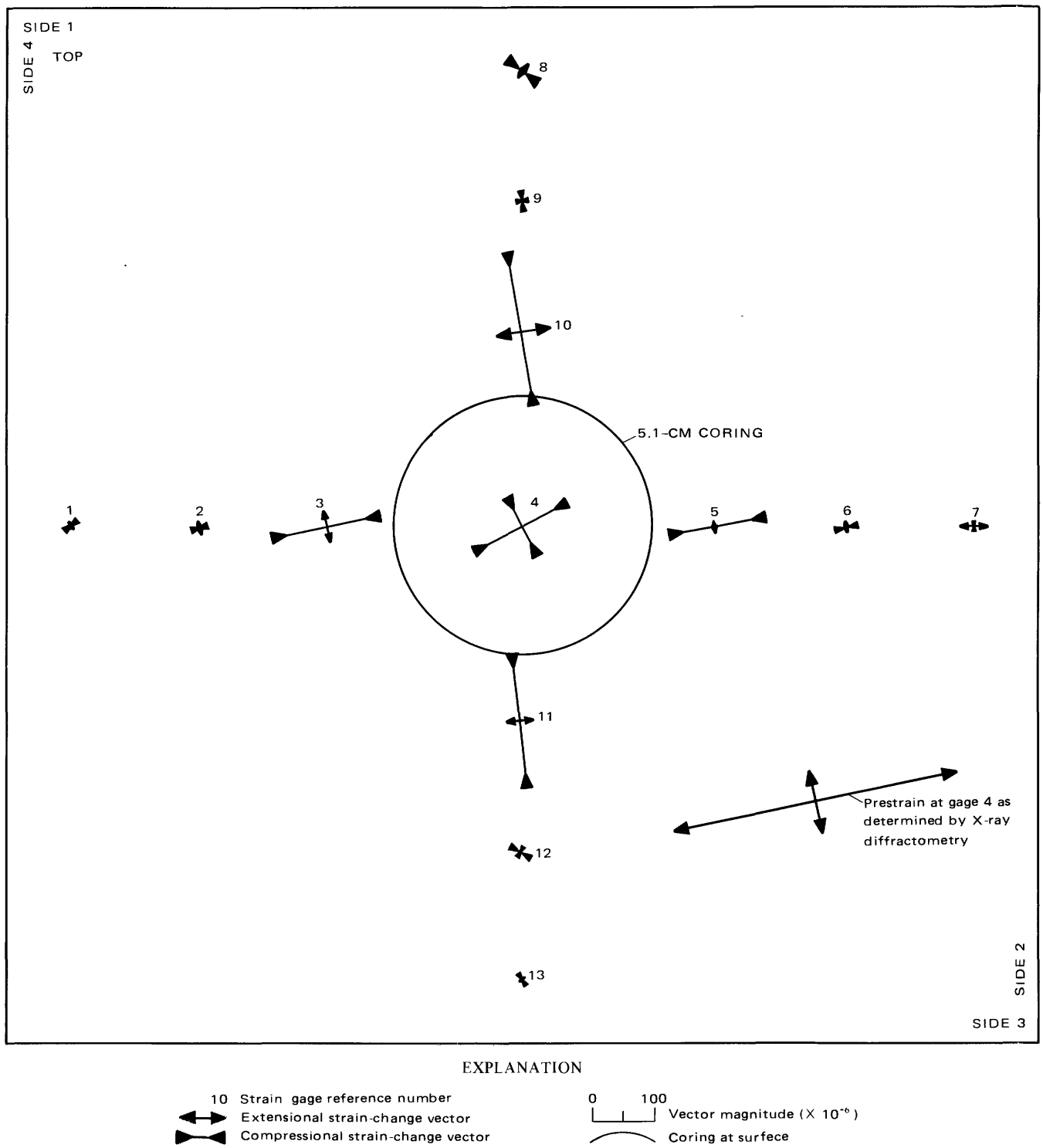

FIGURE 6. — Vectors of principal strain changes $\Delta_0\epsilon_1$ and $\Delta_0\epsilon_2$ on the top surface caused by top 5.1-cm coring (changes that occurred between the time of the initial reading, prior to coring of the top surface, and the top 5.1-cm coring).

tom. With one exception, the $\Delta_0\epsilon_2$ are nearly vertical, and the $\Delta_0\epsilon_1$ are nearly horizontal.

3. $\Delta_0\epsilon$ on the top, bottom, and side 2 after the 15.0-cm coring on top (fig. 8). Twenty-four hours after the 15.0-cm cut, the largest $\Delta_0\epsilon$ are still on the top surface (fig. 8*B*), and all the $\Delta_0\epsilon_2$ are compressive, with magnitudes as large as -275×10^{-6}. The $\Delta_0\epsilon_1$ are both compressive and extensional, with magnitudes as large as $90 \times$

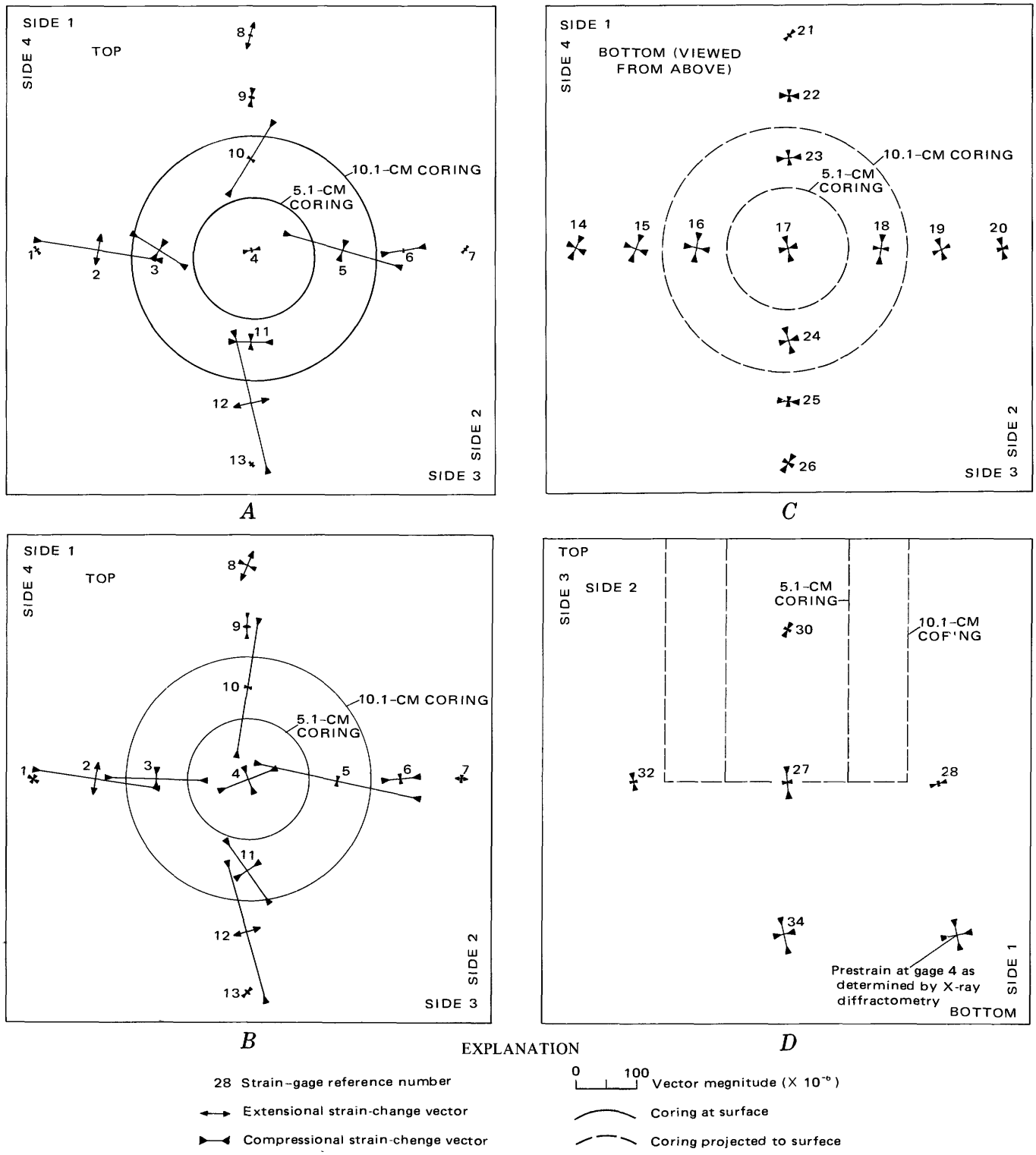

FIGURE 7. — Vectors of principal strain changes after top 10.1-cm coring. *A*, Top surface. Principal strain changes $\Delta\epsilon_1$ and $\Delta\epsilon_2$ (changes occurring in the time between the stable reading (5.1-cm coring) prior to the 10.1-cm coring of top surface. *B*, Top surface. Strain changes $\Delta_0\epsilon_1$ and $\Delta_0\epsilon_2$ (changes after the initial reading made prior to coring top surface) after coring. *C*, Bottom surface. Strain changes $\Delta_0\epsilon_1$ and $\Delta_0\epsilon_2$ after coring. *D*, Side-2 surface. Strain changes $\Delta_0\epsilon_1$ and $\Delta_0\epsilon_2$ after coring.

10^{-6}. The orientations of the $\Delta_0\epsilon_2$ and $\Delta_0\epsilon_1$ axes are all nearly radial and tangential, except at gage 13. At gage 4 on the center core and at all gages on the inner annulus, the $\Delta_0\epsilon$ have remained nearly the same.

Small extensional strain changes created by the 15.0-cm coring (fig. 8*A*) are not readily detected on the $\Delta_0\epsilon$ of the inner annulus at gages 3, 11, 5, and 10. On the outer annulus, $\Delta_0\epsilon_2$ increases are largest at gages 6 and 9, which previously showed the smallest $\Delta_0\epsilon_2$ increase after the 10.1-cm coring. Exterior to the cut, the $\Delta_0\epsilon$ remain small in contrast to the large $\Delta_0\epsilon$ found external to previous cuts.

On the bottom and side 2 (figs. 8*C*, 8*D*), the $\Delta_0\epsilon$ were still mostly compressional but much smaller in magnitude than after the 10.1-cm coring, thus indicating that the exterior of the block was extending instead of contracting, as observed previously. The orientations of the $\Delta_0\epsilon$ axes remain approximately the same as they were following the 10.1-cm coring. There is one strain response on the bottom surface at gage 22 that appears to be anomalous. The $\Delta_0\epsilon_2$ and $\Delta_0\epsilon_1$ are both extensional; $\Delta_0\epsilon_1$ is nearly 90×10^{-6}.

Following the 15.0-cm coring, the gages on the top, bottom, and side 2 showed continued creep for 48 hours. Figure 8*E* shows the strains that occurred on the top side of the block during the second 24 hours after the 15.0-cm coring. All the strains are extensional, with the principal strain axes approximately radial and tangential. The radial strain at gage 8 is exceptionally large, about 110×10^{-6}. Compare figures 8*C* and 8*D*, which show the $\Delta_0\epsilon$ on side 2 and on the bottom 24 hours after drilling, with figures 8*F* and 8*G*, which show the same quantities approximately 48 hours after, when all creep had ceased. The $\Delta_0\epsilon$ orientations remained approximately the same in all cases, but extensional strain changes, with one exception, reduced the compressional $\Delta_0\epsilon$ to very small values, approaching the initial strain state prior to disturbing the block. During the observed-creep episode, a continued anomalous extensional-strain response was recorded at gage 22 that had been observed to have anomalous extensional $\Delta_0\epsilon$ after the 12-hour reading.

The annuli and center core were broken out of the block, leaving on the top surface only the strain-gage rosettes 1, 8, 7, 13, Q, and F on the periphery. The block was then turned over, and coring was started in the same sequence on the bottom surface as on the top. The strain changes $\Delta_B\epsilon$ were then referenced to a stable zero reading just prior to the 5.1-cm coring of the bottom surface.

4. $\Delta_B\epsilon$ on the bottom, side 2, and top surfaces after the 5.1-, 10.1-, and 15.0-cm corings on the bottom (fig. 9). The strain changes $\Delta_B\epsilon$ on the bottom side (figs. 9*A*, *B*, *E*) following the 5.1-, 10.1-, and 15.0-cm corings are in many ways similar to those that occurred on the top surface as it was cored.

The strain changes $\Delta_B\epsilon_2$ and $\Delta_B\epsilon_1$ on the bottom center core are both compressive and of similar magnitude to those that were recorded on the central core of the top surface. The orientations, however, are rotated nearly 90°; the $\Delta_B\epsilon_2$ and $\Delta_B\epsilon_1$ axes nearly coincide with $\Delta_0\epsilon_1$ and $\Delta_0\epsilon_2$ axes, respectively.

Like those on top, the largest strains on the bottom occurred nearest to the fresh cuts; the orientations of the $\Delta_B\epsilon_2$ and $\Delta_B\epsilon_1$ axes are radial and tangential, respectively. The $\Delta_B\epsilon_2$ in the peripheral zone are mostly compressive and of magnitudes as large as -145×10^{-6} (fig. 9*C*, gage 25); the $\Delta_B\epsilon_1$ are nearly all extensional and of magnitudes as large as 145×10^{-6} (fig. 9*C*, gage 26). The compressive $\Delta_B\epsilon_2$ induced by the cuts on the bottom surface are much less compressive than the $\Delta_0\epsilon_2$ on the top surface, and the $\Delta_B\epsilon_1$ are much more extensional than are the $\Delta_0\epsilon_1$. The $\Delta_B\epsilon_1$ on the peripheral surface external to the 15.0-cm cut are especially large, indicating that the exterior rind of the block is expanding.

The $\Delta_B\epsilon_2$ and $\Delta_B\epsilon_1$ on side 2 and at the remaining two good gages (7 and 13) on top (figs. 9*E*, *D*, respectively) corroborate the expansion of the exterior rind. The $\Delta_B\epsilon_2$ are mostly extensional or slightly compressional, whereas the $\Delta_B\epsilon_1$ are all extensional, and the orientations have remained nearly the same as they were after coring the top surface — that is, vertical and horizontal on side 2, radial and tangential on top. Maximum magnitudes of extensional strain are 90×10^{-6} (fig. 9*D*, gage 7), and maximum magnitudes of compressional strain are -15×10^{-6} (fig. 9*D*, gage 30). The smallest $\Delta_B\epsilon$ on side 2 are in the middle (gages 27, 28, and 32), nearest to the thin interior rock plate still connecting the annuli to the main rock mass.

After the bottom was completely cored, the center core was broken out, and an attempt was made to break the annuli away from the thin rock plate at the bottom of the cut. The annuli did not break; instead, three small chips were broken away from the central annulus, resulting in the strain changes shown in figure 9*F*. At the gage locations (16, 23, and 24) on the freed chips and near the new break, there are large strain changes, both extensional and compressional, from 200×10^{-6} to -150×10^{-6}. Smaller changes occur on the still-intact protion of the annulus at gage 18. Also, a small change occurs on the outer annulus adjacent to one of the fractured chips at gage 22.

5. $\Delta_B\epsilon$ on the bottom, side-2, and top surfaces after the 10.1-cm coring on side 2 (fig. 10). The block was then rotated, and side 2 was cored with the 10.1-cm core bit to a depth of 12.0 cm, partially relieving the thin rock plate still holding the bottom annuli. Resulting strain changes $\Delta_B\epsilon$, referenced to the zero reading established prior to coring the bottom, are shown in figures 10*B*, *C*, and *D*. On the bottom surface the orientations of the $\Delta_B\epsilon_2$ and $\Delta_B\epsilon_1$ axes remained approximately the same, but in most places the $\Delta_B\epsilon_2$

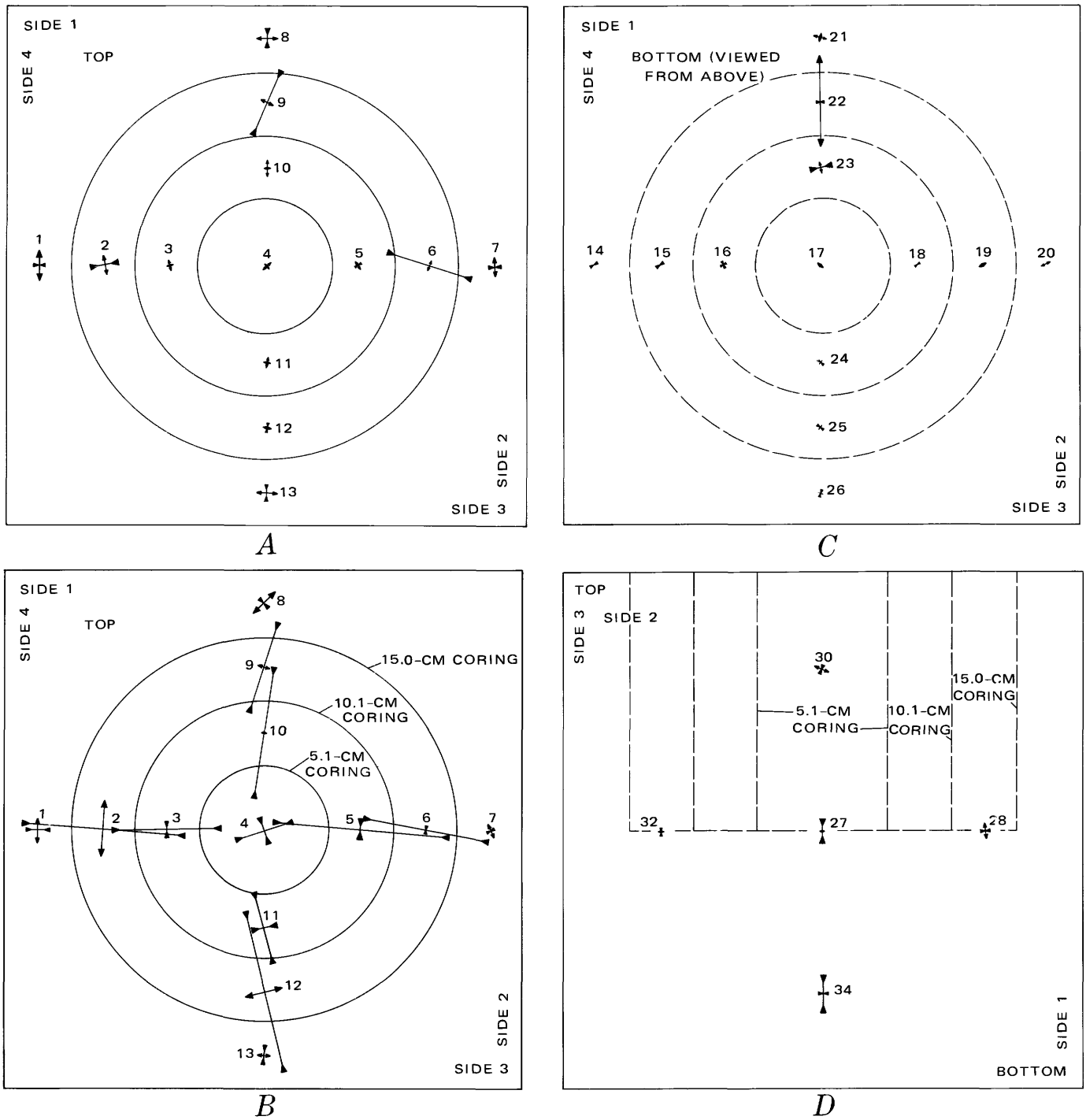

FIGURE 8. — Vectors of principal strain changes after top 15.0-cm coring. *A*, Top surface. Principal strain changes $\Delta\epsilon_1$ and changes $\Delta_0\epsilon_1$ and $\Delta_0\epsilon_2$ (changes since the initial reading made prior to coring top surface) 24 hours after coring. *C*, hours after coring. *E*, Top surface. Principal strain changes $\Delta\epsilon_1$ and $\Delta\epsilon_2$ (changes since the 24 hour reading) 48 hours surface. Strain changes $\Delta_0\epsilon_1$ and $\Delta_0\epsilon_2$ 48 hours after coring.

axes decreased in compression, and the $\Delta_B\epsilon_1$ axes increased in extension.

Similarly, on side 2 the orientations of the $\Delta_B\epsilon$ remained nearly identical, but the magnitudes, especially of the $\Delta_B\epsilon_1$, changed somewhat. Radial $\Delta_B\epsilon_2$ changed very little; either they became slightly more compressive or slightly more extensional, whereas the tangential $\Delta_B\epsilon_1$ have all increased in extension to magnitudes of nearly 100×10^{-6} (gage 30). On the central core at gage 27 the compressional $\Delta_B\epsilon_2$ and the

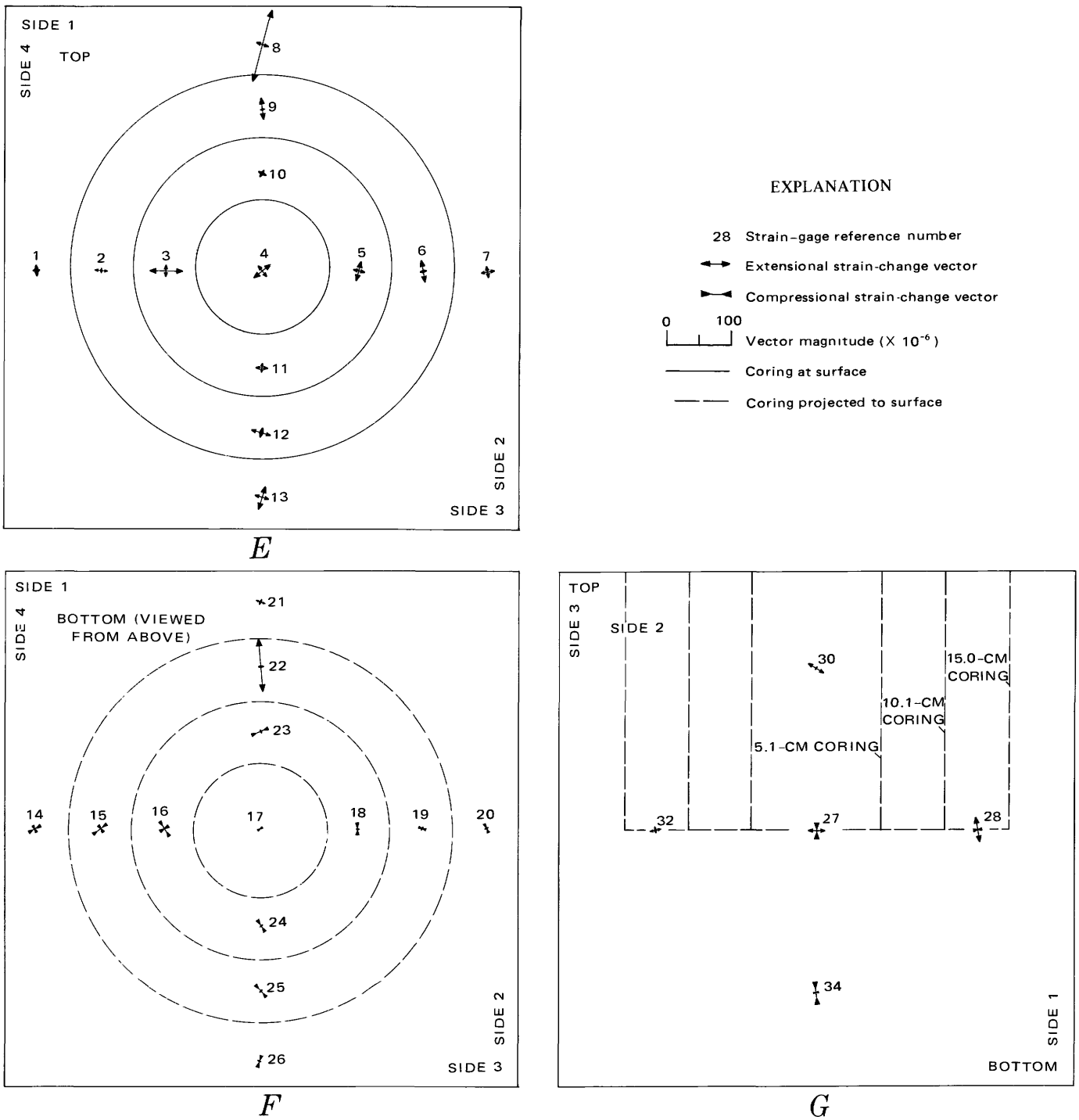

$\Delta\epsilon_2$ (changes since the stable reading made prior to the coring) 24 hours after the 15.0-cm coring. *B*, Top surface. Strain Bottom surface. Strain changes $\Delta_0\epsilon_1$ and $\Delta_0\epsilon_2$ 24 hours after coring. *D*, Side-2 surface. Strain changes $\Delta_0\epsilon_1$ and $\Delta_0\epsilon_2$ 24 after the same coring (creep event). *F*, Bottom surface. Strain changes $\Delta_0\epsilon_1$ and $\Delta_0\epsilon_2$ 48 hours after coring. *G*, Side-2

extensional $\Delta_B\epsilon_1$ axes are, respectively, vertical and horizontal.

On the top surface the orientations of $\Delta_B\epsilon_2$ and $\Delta_B\epsilon_1$ have rotated slightly, but they still remain nearly radial and tangential to the original 15.0-cm core hole. Both $\Delta_B\epsilon_2$ and $\Delta_B\epsilon_1$ have become largely extensional, with magnitudes as large as 145×10^{-6} (gage 7).

To demonstrate more clearly the geometric effect of the freshly cut surfaces, three additional gages (29, 31, and 33) were placed radially on side 2 (along with

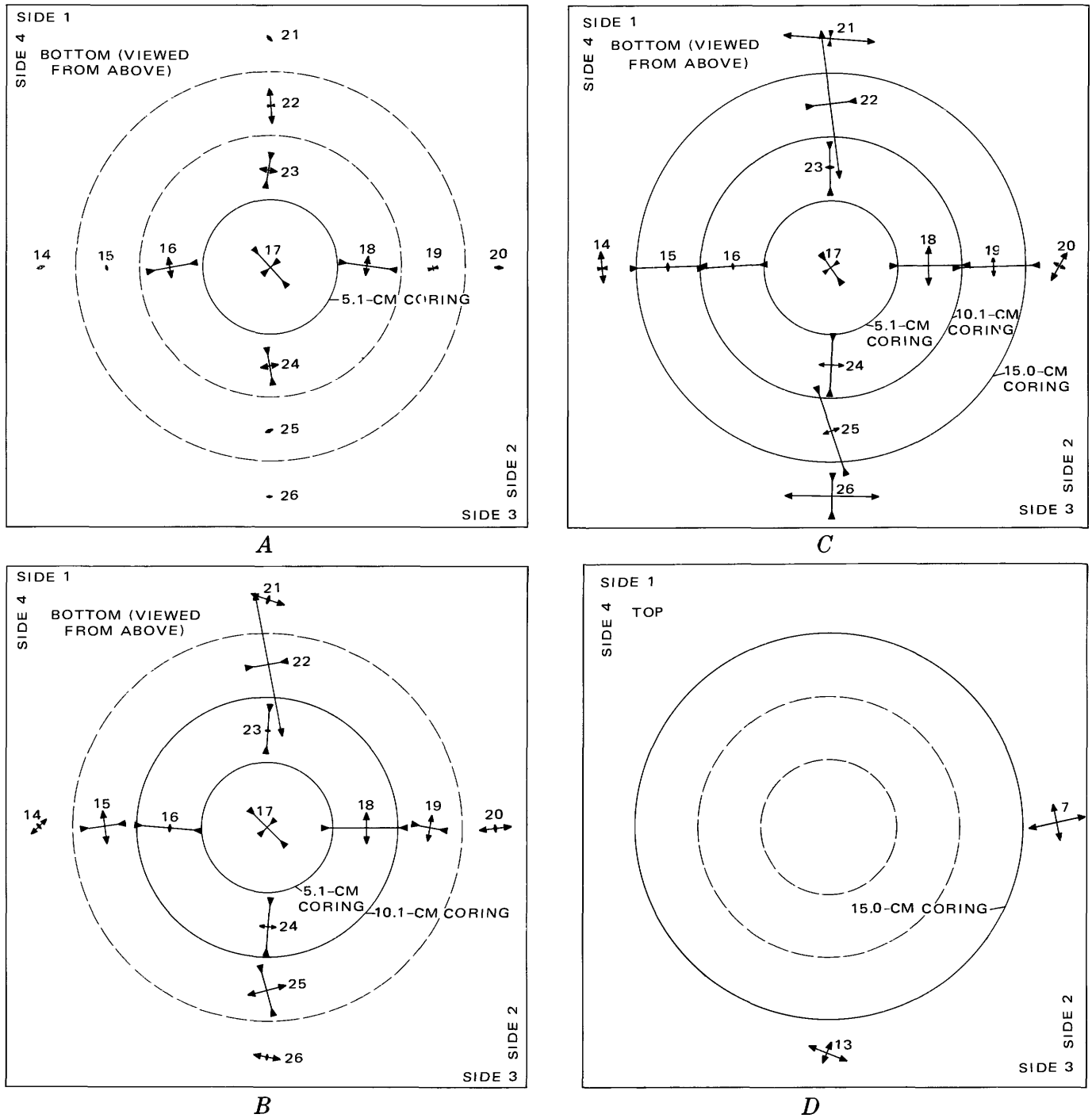

FIGURE 9. (above and facing page). — Vectors of principal strain changes caused by bottom coring. *A*, Bottom surface. Strain changes $\Delta_B \epsilon_1$ and $\Delta_B \epsilon_2$ (changes after stable reading made prior to coring bottom surface) after bottom 5.1-cm coring. *B*, Bottom surface. Strain changes $\Delta_B \epsilon_1$ and $\Delta_B \epsilon_2$ after bottom 10.1-cm coring. *C*, Bottom surface. Strain changes $\Delta_B \epsilon_1$ and $\Delta_B \epsilon_2$ after bottom 15.0-cm coring. *D*, Top surface. Strain changes $\Delta_B \epsilon_1$ and $\Delta_B \epsilon_2$ after bottom 15.0-cm coring. *E*, Side-2 surface. Strain changes $\Delta_B \epsilon_1$ and $\Delta_B \epsilon_2$ after bottom 15.0-cm coring. *F*, Bottom surface. Strain changes $\Delta \epsilon_1$ and $\Delta \epsilon_2$ caused by chipping interior annulus. Strain changes determined from equilibrium state prior to chipping.

gages 28, 30, 32, and 34) prior to the 10.1-cm coring. Figure 10*A* shows the principal strain changes that occurred at these seven gage locations from immediately before to 12 hours after the 10.1-cm cut. External to the cut (gages 28 through 34), the minimum principal strain changes are entirely radial, and the maximum principal strain changes are tangential. The magnitudes and senses of strain changes very con-

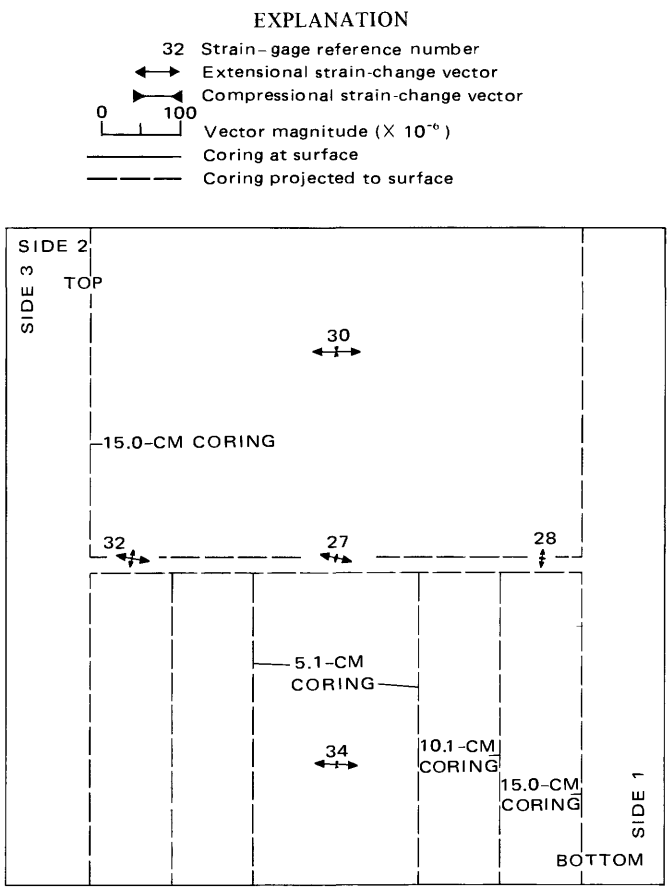

siderably, but the orientations remain consistent with the geometry of the cut. The maximum principal strain changes are all extensional and range from 10×10^{-6} to 60×10^{-6}, whereas the minimum principal strain changes are generally small extension or compression (less than 10×10^{-6}), except for one compressional value of -55×10^{-6}.

6. Total strain changes $\Delta'_0\epsilon = \Delta_0\epsilon + \Delta_B\epsilon$ on the bottom, side-2, and top surfaces after all drilling was completed (fig. 11). The 10.1-cm coring on side 2 completed the drilling program, after which final calculations of the principal strain changes $\Delta'_0\epsilon_2$ and $\Delta'_0\epsilon_1$ were made for the total duration of the experiment — that is, strain changes were determined from the time of the initial reading prior to the first overcore on top to the final stable reading after the 15.0-cm coring on side 2. Figure 11 shows these total principal strain changes at the locations where the strain gages were still recording.

   On the bottom surface (fig. 11*B*), the total principal strain changes $\Delta'_0\epsilon_2$ and $\Delta'_0\epsilon_1$ on the cored annuli are radically compressional and tangentially extensional, with one exception. At gage 22 on the outer annulus, toward side 1, the $\Delta'_0\epsilon_2$ (-50×10^{-6}) is compressional and tangential, and the $\Delta'_0\epsilon_1$ (360×10^{-6}) is extensional and radial.

   At gage locations (4, 20, 21, and 26) external to the annuli, the $\Delta'_0\epsilon$ are mostly extensional and tangential, indicating circumferential expansion of the outside rind. The radial strains at these locations are very small.

   The total compressional strain magnitudes are as much as -115×10^{-6} (gage 15), and the extensional strain magnitudes were as much as 370×10^{-6} (gage 22).

   On side 2 (fig. 11*C*,) the $\Delta'_0\epsilon_2$ external to the 10.1-cm cut are radial and mostly compressional. The $\Delta'_0\epsilon_2$ at gage 32 is extensional. The corresponding $\Delta'_0\epsilon_1$ are all extensional and tangential. Magnitudes of the compressional $\Delta'_0\epsilon_2$ are as much as -80×10^{-6} (gage 34), and magnitudes of the extensional $\Delta'_0\epsilon_1$ are as much as 105×10^{-6} (gage 30). On the center core, $\Delta'_0\epsilon_2$ is compressional and vertical, and $\Delta'_0\epsilon_1$ is extensional and horizontal.

   On the top surface (fig. 11*A*) at the remaining locations external to the cut, the total $\Delta'_0\epsilon$ are entirely extensional, nearly radial and tangential, and with magnitudes as large as 130×10^{-6} (gage 7).

7. $\Delta\epsilon$ on the quartz and feldspar grains after the 10.1 and 15.0-cm corings on the top and after the 5.1-cm coring on the bottom (figs. 12, 13). Figure 12 shows the principal strain changes that took place on the individual feldspar (F_1,F_2) and quartz (Q) grains after the 10.1- and 15.0-cm corings on top and, finally, 48 hours after the 15.0-cm coring on top. These changes refer back to an initial reading taken after the 5.1-cm but before the 10.1-cm coring.

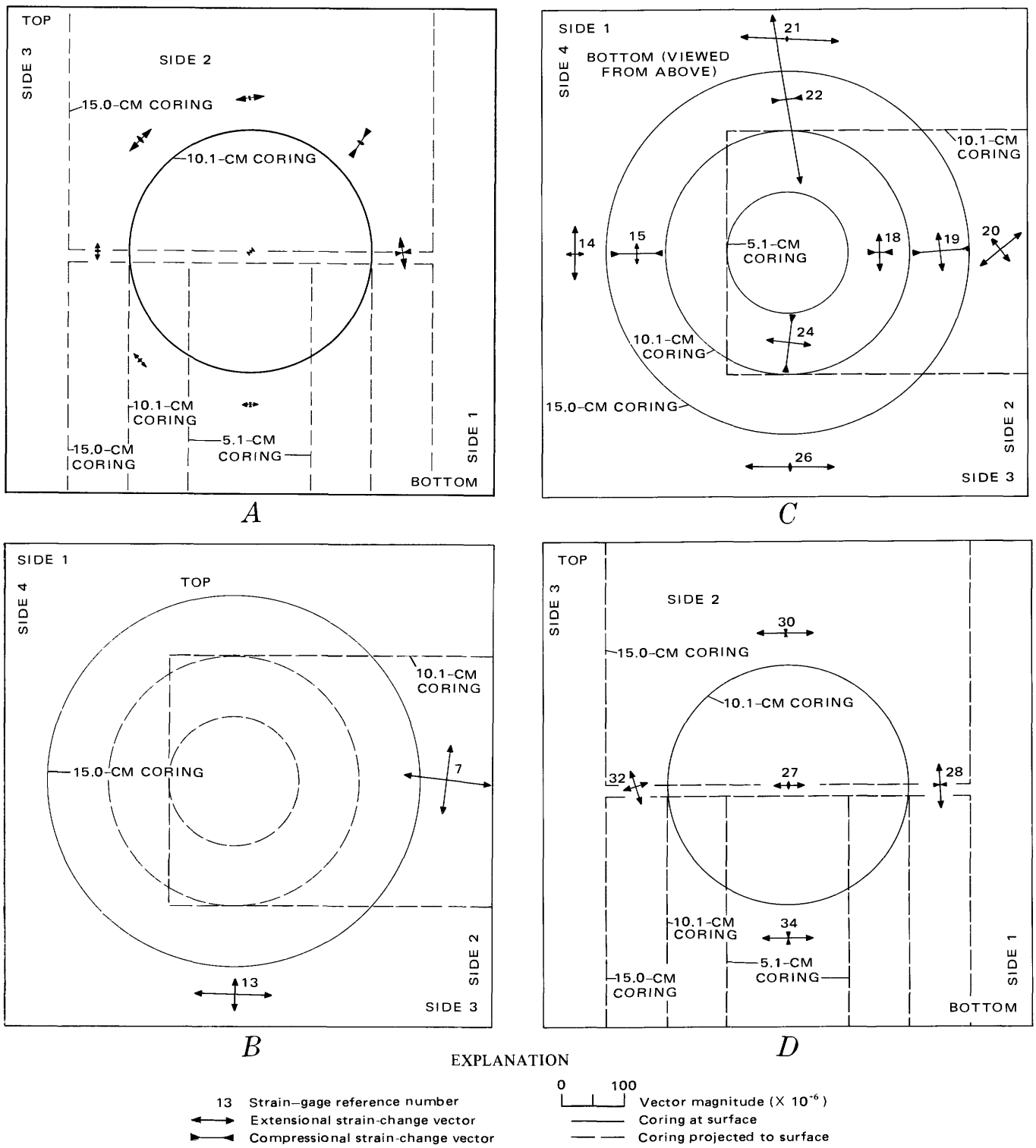

FIGURE 10. — Vectors of principal strain changes caused by side-2 10.1-cm coring. *A*, Side-2 surface. Strain changes $\Delta\epsilon_1$ and $\Delta\epsilon_2$ after the stable reading prior to the side-2 10.1-cm coring. *B*, Top surface. Strain changes $\Delta_B\epsilon_1$ and $\Delta_B\epsilon_2$ (changes after stable reading prior to coring bottom surface). *C*, Bottom surface. Strain changes $\Delta_B\epsilon_1$ and $\Delta_B\epsilon_2$. *D*, Side-2 surface. Strain changes $\Delta_B\epsilon_1$ and $\Delta_B\epsilon_2$.

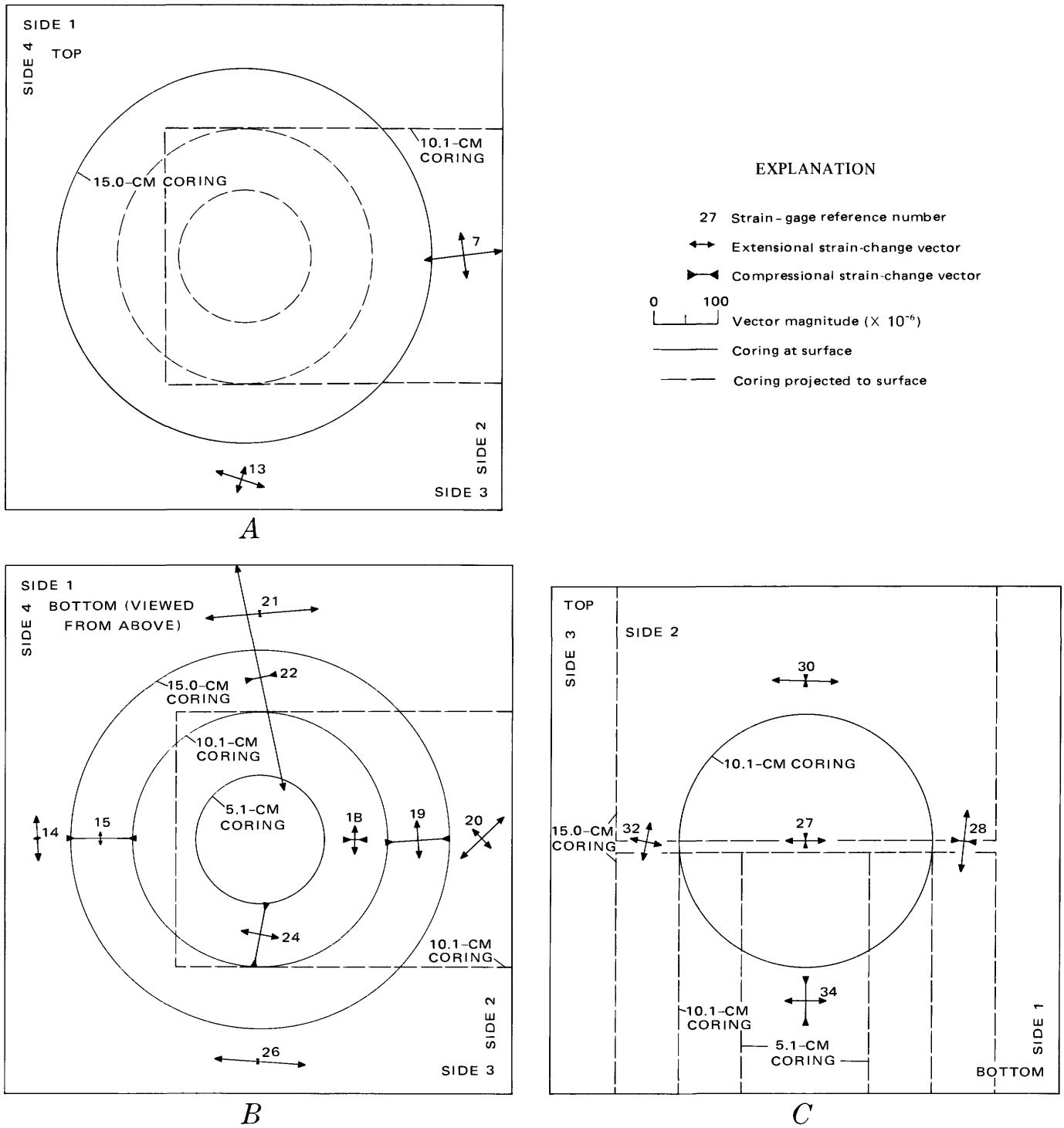

FIGURE 11. — Vectors of total net strain changes $\Delta'_0\epsilon_1$ and $\Delta'_0\epsilon_2$ (total strain change for experiment) after 10.1-cm coring on side 2. *A*, Top surface. *B*, Bottom surface. *C*, Side-2 surface.

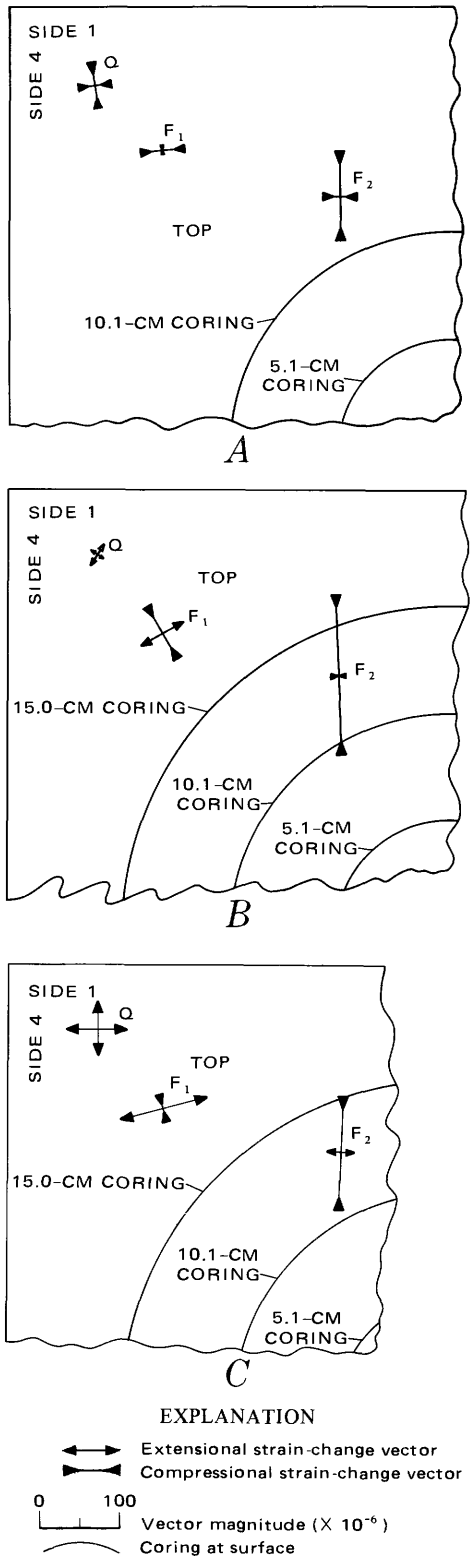

FIGURE 12. — Vectors of principal strain changes on quartz (Q) and feldspar F_1, F_2) grains on the top surface after 10.1-cm and 15.0-cm coring on the top surface but references to the stable reading after the 5.1-cm coring. *A*, Changes measured after the 10.1-cm coring. *B*, Changes measured 24 hours after the 15.0-cm coring. *C*, Changes measured 48 hours after the 15.0-cm coring.

FIGURE 13. — Vectors of principal strain changes $\Delta_B\epsilon_1$ and $\Delta_B\epsilon_2$ ▷ (strain changes after stable reading made prior to coring bottom) over quartz (Q) and feldspar (F_1) grains on top surface. *A*, 24 hours after the 5.1-cm coring on the bottom face. *B*, 41 days after the 5.1-cm coring on the bottom face. *C*, 24 hours after the 10.1-cm on the bottom face.

Figure 13 shows the strain changes on the same gages which took place during the 5.1- and 10.1-cm corings on the bottom. The initial reading was just prior to the bottom 5.1-cm coring.

Following the 10.1-cm corings on the top (fig. 12*A*), the principal strain changes in individual quartz and feldspar grains are all compressional but are not obviously radial or tangential. The magnitudes (as much as -80×10^{-6}) tend to get smaller with distance outward from the fresh cut.

At the 12-hour reading following the 15.0-cm coring (fig. 12*B*), the quartz and feldspar locations external to the cut have $\Delta\epsilon$ are radial, and the $\Delta\epsilon_1$ are tangential. The $\Delta\epsilon_2$ at gage F_1 becomes much larger in compression (-55×10^{-6}), whereas the $\Delta\epsilon_2$ at gage Q and the $\Delta\epsilon_1$ at both gages Q and F_1 become more extensional (as large as 50×10^{-6}).

During the same interval, the $\Delta\epsilon$ at gage F_2 on the outer annulus does not change much in orientation, but the $\Delta\epsilon_2$ becomes larger in compression (-150×10^{-6}), and the $\Delta\epsilon_1$ is smaller in compression (-15×10^{-6}).

After the 15.0-cm coring, both the quartz and the feldspar gages recorded significant creep. Figure 12*C* shows the strain changes after creep had ceased at 48 hours, indicating slight to moderate extensional changes in all directions and some rotation of the $\Delta\epsilon$ orientations on the quartz grain.

Twenty-four hours after the 5.1-cm coring on the bottom, thequartz and feldspar grains showed increased extensional strains (fig. 13*A*). The strain changes, $\Delta_B\epsilon_2$ and $\Delta_B\epsilon_1$, with respect to the bottom zero readings are both extensional; the $\Delta_B\epsilon_1$ at gage F_1 is large (131×10^{-6}). The orientations of the $\Delta_B\epsilon_2$ and $\Delta\epsilon_1$ axes, however, are not tangential or radial.

A creep event occurred at gages Q and F_1 for 41 days after the 5.1-cm bottom overcore. Figure 13*B* shows the $\Delta_B\epsilon$ of the quartz and feldspar grains (gages Q and F_1) after 41 days, and the creep had ceased. Both the feldspar and the quartz grains show compressional creep changes, with rotations of orientations of $\Delta\epsilon_2$ and $\Delta\epsilon_1$.

After the 10.1-cm coring on the bottom, the strain changes, $\Delta_B\epsilon_1$ and $\Delta_B\epsilon_2$, at the quartz and feldspar grains are again highly extensional, with magnitudes as large as 181×10^{-6} (fig. 13*C*). The orientations of $\Delta_B\epsilon_1$ and $\Delta_B\epsilon_2$ are nearly the same as they were after the 5.1-cm coring on the bottom.

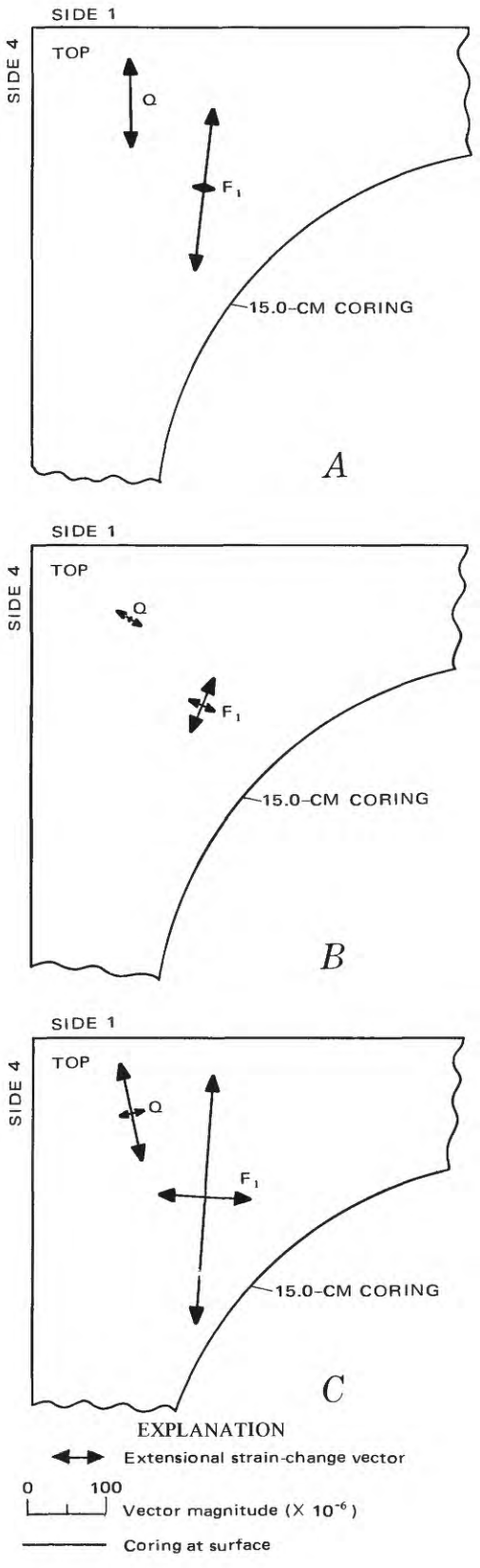

PHASE II

SURFACE FABRIC CHANGES

Figures 14*A* and *C* show enlarged photographs of surface areas that were decorated with organic dyes prior to coring the block. The area in figure 14*A* is 14.5 cm from the center and midway between gages 6 and 9 (a location of high strain response), and the area in figure 14*C* is 16.9 cm from the center and midway between gages 7 and 8 (low strain response). Figures 14*B* and *D* show the same areas after the coring on the top surface was finished. upon comparing fabric elements at both locations before and after coring, one finds no obvious changes except immediately adjacent to the fresh surface seen in figure 14*B*. The development of a zone of microfracturing about 1 mm thick can be inferred by the higher intensity of refracted light. This zone of microfracturing was corroborated by thin-section examination. Elsewhere, the microfractures seen in these photographs can be identified in nearly every case both before and after coring. In a few cases the fractures may appear to be wider from one photograph to another, but this difference may be caused by either crack displacement or difference in the intensity of reflected light.

PHASE III

ANISOTROPY OF PETROFABRIC ELEMENTS

Figure 15 shows photomicrographs of microfractures in the lift and rift planes. Open and healed fractures, seen as linear elements on the lift plane, are parallel to the rift plane (fig. 15*A*), and similar fractures, seen as linear elements in the rift plane, are, in turn, parallel to the lift plane (fig. 15*B*). These fracture sets have very strong preferred orientations parallel to both planes; the most dense fracture set is parallel to the lift plane.

OTHER SIGNIFICANT PETROFABRIC FEATURES

Other fabric features observed are the large numbers of quartz grains with undulatory extinction and clusters of small quartz and feldspar grains along larger grain boundaries that indicate some degree of recrystallization.

Examination of two sets of orthogonal thin sections, one taken from a highly strained area (figs. 14*A, B*) and the other from a moderately strained area (figs 14*C, D*), reveals no changes of fracture spacing or orientations that would indicate any incipient fracture development upon overcoring and strain relief.

DISCUSSION

STRAIN MAGNITUDES

The strain data obtained by successively creating new axially symmetrical surfaces within a 22-cm cube of Barre Granite suggest that rock masses can store a significant amount of residual stress that is capable of being unlocked or mobilized over large areas in a complex manner. The block released principal strain

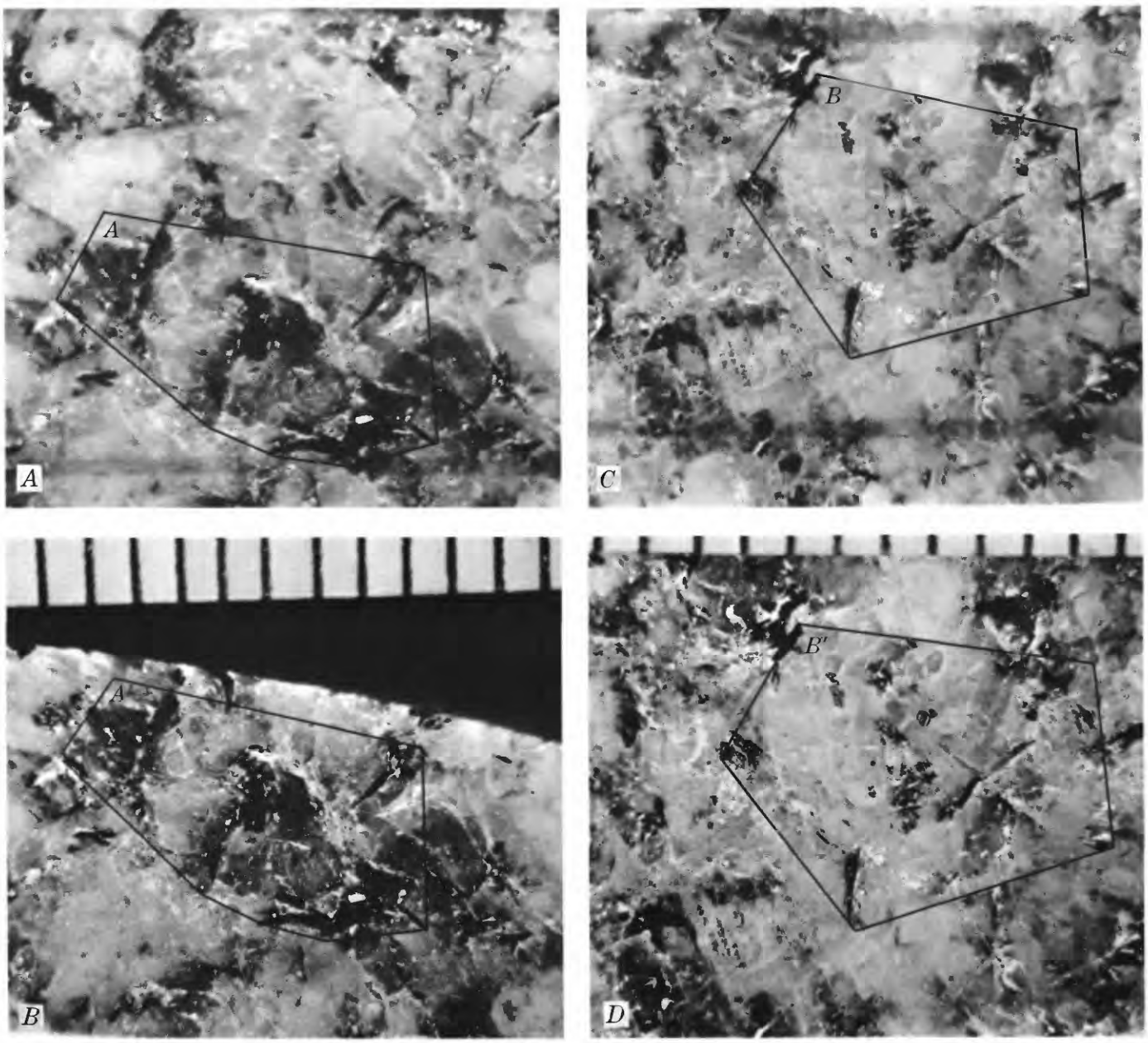

FIGURE 14. — Reflected-light photographs of surfaces dyed with organic fluorescent dye before and after coring. Areas A and A' are identical, as are areas B and B'. Scale divisions, 1 mm. A, Location on outer annulus between gages 9 and 6; before coring. B, Same location as A, after coring. A large number of new fractures occur within the first 2 mm from the cut. Otherwise no new fractures can be identified. C, Location 2.5 cm radially exterior to the location in A; before coring. D, Same location as in C, after coring. No new fractures can be identified.

changes as much as -275×10^{-6} (compression) and 330×10^{-6} (extension) on newly cut surfaces.

BEHAVIOR OF THE BLOCK — CORING OF TOP SURFACE

As the top of the block was cored successively outward, the strain changes adjacent to the fresh surfaces became highly compressional in radial directions but became only slightly compressional or slightly extensional in circumferential directions. The principal strain changes within 2 cm of both sides of the circular cuts all had nearly the same sense, orientation, and magnitude; strain changes on the outer skin (rind) were much less compressional. Forty-eight hours after the top 15.0-cm coring, these strains had returned nearly to the precoring strain conditions.

On the bottom and side 2, all strain changes were moderately compressional after the 10.1-cm coring, but they had recovered to nearly zero 48 hours after the 15.0-cm coring. The largest strain changes (near the bottom of side 2, gage 32) agree very well with adjacent strain

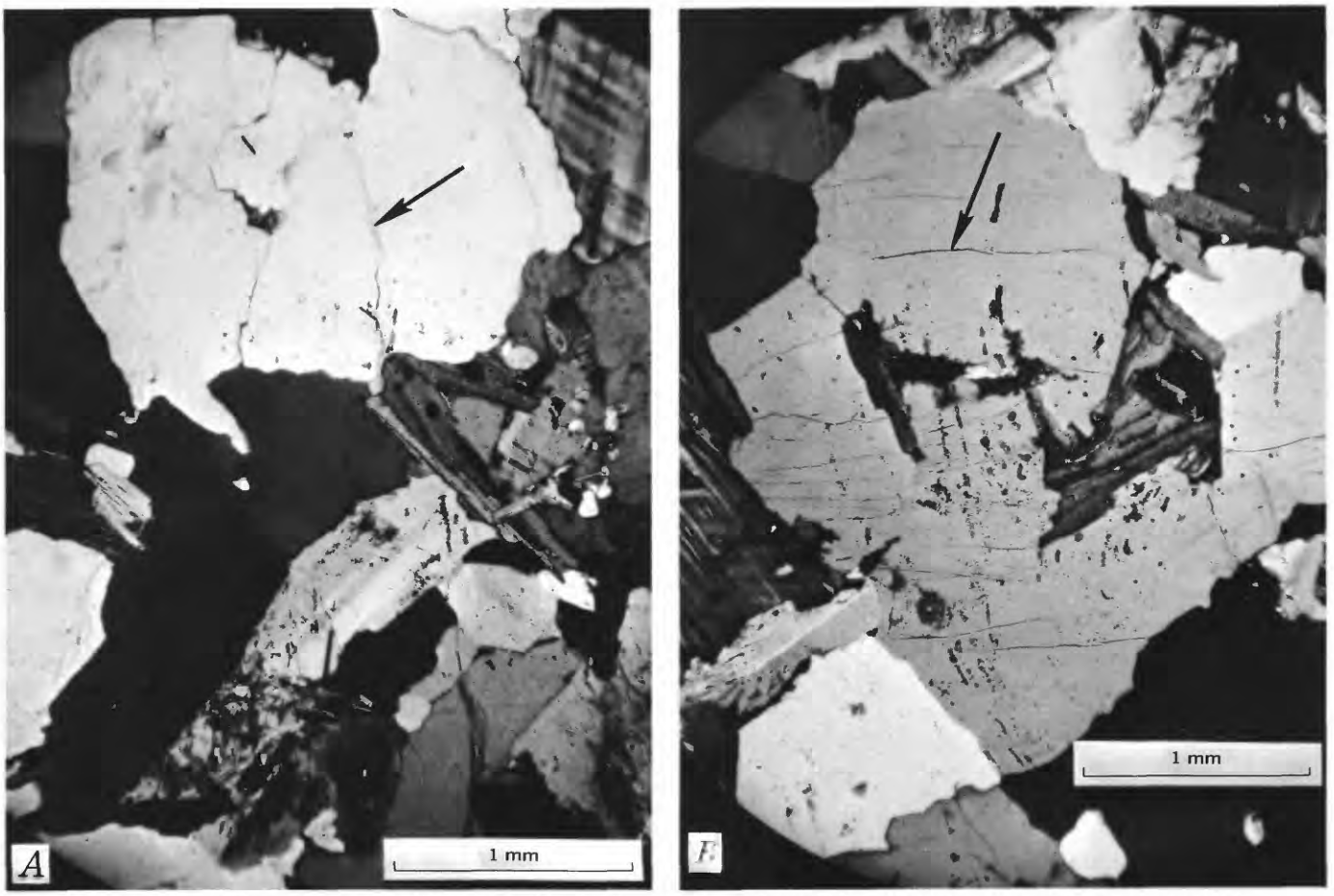

FIGURE 15. — Photomicrographs of Barre Granite. *A*, Fractures (arrow) parallel to rift plane; plane of photomicrograph is parallel to lift plane. *B*, Fractures parallel to lift plane; plane of photomicrograph is parallel to rift plane.

changes in the same direction on the bottom surface (gage 20), whereas smaller strain changes toward the top of side 2 (gage 30) agree very well with adjacent strain changes in the same direction on the top surface (gage 7).

Thus, as coring proceeded, the block deformed in a manner related primarily to the geometry of the newly created surfaces, the initial shape of the block, and the release of available residual stress.

BEHAVIOR OF THE TOP SURFACE

After the initial 5.1-cm drilling, the central core deformed elliptically, as would be expected of a cylinder cut from a mass having a prestress that was nonhydrostatic. The circular cut allowed equal degrees of freedom for deformations in all directions normal to the circular axis, so that the strains should reflect the state of prestress.

After the 10.1- and 15.0-cm corings, the large compressive radial strains within the annuli indicate that each annulus became thinner. The tangential strains were small. The inferred net circumferential deformation on the middle circumference of the innner annulus, based on tangential strains, is compressional, whereas the net circumferential deformation on the middle circumference of the outer annulus is extensional. using the average radial and tangential strains on each annulus at the middle circumference, one can calculate the radial displacements from the formulas for radial and tangential infinitesimal strain, from McClintock and Argon (1966, p. 60).

$$\epsilon_{rr} = \frac{\partial U_r}{\partial_r} ,$$

and

$$\epsilon_{\theta\theta} = 1/r \frac{\partial U_\theta}{\partial \theta} + \frac{U_r}{r} ,$$

where

ϵ = average radial strain,
$\epsilon_{\theta\theta}$ = average tangential strain,
U_r = radial displacement,
U_θ = tangential displacement, and
r = mean radius.

If the annuli remain circular during deformation, then

$$U_\theta = \text{constant},$$

and

$$\frac{\partial U_\theta}{\partial_\theta} = 0.$$

Thus,

$$U_r = r\epsilon_{\theta\theta}.$$

For the inner annulus, at gages 3, 5, 10, and 11, the average

$$\epsilon_{\theta\theta} = -24 \times 10^{-6},$$

$$U_r = 3.80\ (-24 \times 10^{-6}) = -91 \times 10^{-6}\ \text{cm}.$$

For the outer annulus, gages 2, 6, 9, and 12, the average

$$\epsilon_{\theta\theta} = 39 \times 10^{-6},$$

so

$$U_r = 6.35\ (39 \times 10^{-6}) = 245 \times 10^{-6}\ \text{cm}.$$

Thus, the middle circumferences of both annuli have been radially deformed, the inner annulus by -91×10^{-6} cm, and the outer annulus by 245×10^{-6} cm. These deformations are based on the assumption that the annuli remain circular as they deform, which they obviously do not. The intent is merely to give the reader some feel for how on the average, the annuli surfaces are being displaced relative to the center of the top surface.

The strains, created by relief of the prestress, must be contained within the body of the annuli, where the least constraint is radial and the maximum constraint of freedom is circumferential. Thus, upon relieving the residual stress field, the geometry of the new surfaces control the release of stress such that the radial strain components are the greatest, and the circumferential strain components are the least. The nonhydrostatic aspect of the residual stress field is suggested by the varied magnitudes of strain changes both in radial and circumferential directions, and also by the unequal principal strain changes on the central core. Also, the varied magnitudes in part may be related to the thickness of the annuli. In table 3 the annulus thickness and magnitude of $\Delta_0\epsilon_2$ are given at each gage site. In general, where the annuli are thinnest the magnitudes are largest, but there are exceptions that cast some doubt on this relationship. When the total thicknesses of the annuli are summed in the direction of gages 9 and 12 and then in the direction of gages 2 and 6, the sums are, respectively, 8.265 cm and 8.313 cm. Yet the average $\Delta_0\epsilon_2$ for these same directions are, respectively, -181×10^{-6} and -224×10^{-6}, suggesting that the total thickness of both annuli may not be as significant as other factors (such as anisotropy of the internally stored energy) in controlling strain magnitudes.

On the top surface the strain changes never became highly compressional at gages 1, 7, 8, and 13 on the outer edge (rind). After the 10.1- and 15.0-cm corings were made, the rind experienced very small radial and circumferential strains. The average circumferential strain from gages 1, 7, 8, and 13, $\epsilon_{\theta\theta} = 28 \times 10^{-6}$, was used to calculate the radial displacement of the rind, $U_r = 249 \times 10^{-6}$ cm. Thus, the rind increased in radius about the same as the outer annulus.

TABLE 3. — *Magnitude of $\Delta_0\epsilon_2$ and respective thicknesses of annuli after 15.0-cm overcoring on the top surface. The $\Delta_0\epsilon_2$ and annuli thicknesses are shown for each gage location on the annuli surfaces.*

Gage No.[1]	Annulus		$\Delta_0\epsilon$ 24 hours after 15.0-cm overcoring ($\times 10^{-6}$)
	Inner or outer	Thickness (cm)	
12	Outer	1.912	−255
5	Inner	1.925	−274
2	Outer	1.933	−257
10	Inner	1.966	−206
9	Outer	2.046	−149
6	do	2.060	−198
11	Inner	2.341	−113
3	do	2.395	−166

[1]Listed in order of thickness of annulus.

BEHAVIOR OF SIDE-2 AND BOTTOM SURFACES

The side-2 and bottom faces can be regarded as part of the external rind relative to the coring of the top surface. The strains on these faces, especially those on the lower half of the block that attained their greatest magnitude after the 10.1-cm coring, are smaller and much more uniform than those on the top face. The bottom face indicates nearly equal strain changes at most of the locations monitored, and the axes of the principal strain changes reflect the orientations of the axes of these principal strain changes on the top surface. The strains seen on the bottom outer rind apparently reflect an interior stress state created by the coring procedure. If the strains caused by cutting a uniform residual stress field are uniformly distributed down the cylindrical annulus segment to the base of the cut, one can imagine a cylindrical cantilever type of loading (fig. 16) applied through these segments to the lower half of the rock. The still-intact lower rind responds with diminished but uniform strains that reflect the cantilever loading. On the other hand, the rind of the upper half of the block is attached to the lower rock mass only at the base of the 10.1-cm cut. The very small strain changes on the upper rind are attributed to the combination of relieved stresses adjacent to the newly cut surface and the cantilever stresses distributed through the attachment zone.

After the 15.0-cm coring and associated creep event, the surfaces on the lower half of the rock recovered extensionally to nearly the precoring condition of strain. The upper exterior rind, made thinner by coring, recovered to the initial state and then became very slightly extensional. Thus, it appears that the combined

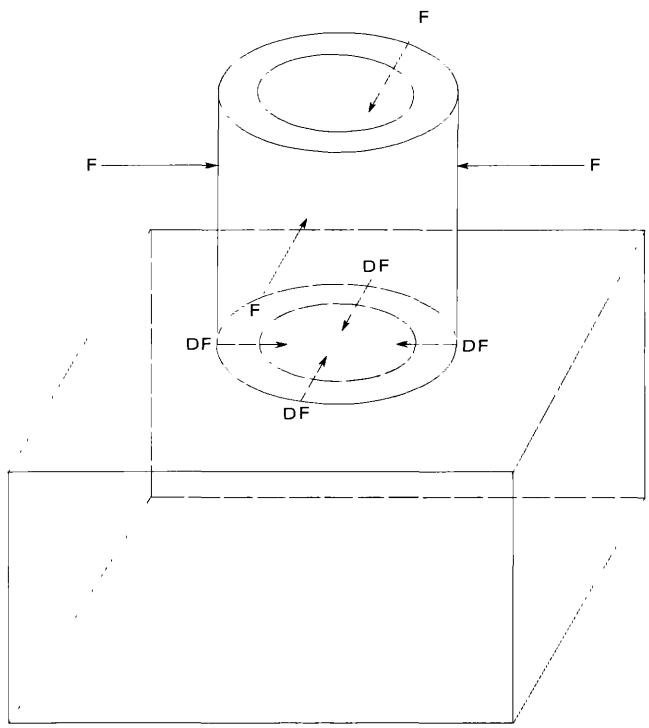

FIGURE 16. — A cylindrical cantilever oriented vertically upon a block. The moment caused by gravity loading is equal to zero. Applied forces (F) on boundary are distributed through the base onto the block as shown by arrows DF.

interaction of the internal cantilever stresses and the relieved residual stresses produces a net strain change of nearly zero on the side-2 and bottom surfaces, both being uncut surfaces on the external rind.

BEHAVIOR OF THE BLOCK — CORING OF BOTTOM SURFACE

When the block was turned over and cored on the bottom, the responses were similar — that is, the central 5.1-cm core had all compressive strains having magnitudes similar to those of the central core on the top. The orientations of the principal strain axes were rotated about 70°. The annuli had principal strains oriented radially and tangentially; the radial strains were also compressive but of lesser magnitudes than those on top. However, the tangential strains were nearly all extensional, and they became very large, especially on the exterior rind, as the coring progressed outward. Side 2 became nearly all extensional horizontally, with practically no vertical change, and the exterior rind on the top was highly extensional. Total strains in the quartz and feldspar grains on the top exterior rind were entirely extensional after the 5.1-cm and 10.1-cm corings, and the $\Delta_B\epsilon$ were oriented neither radially nor tangentially, except after the 41-day creep event (fig. 8). During this creep event, the $\Delta_B\epsilon$ became more compressional, and their axes rotated to radial and tangential positions. The creep event noted on these gages was not observed at most of the other gages.

BEHAVIOR OF BLOCK — CORING OF SIDE-2 SURFACE

After the final 10.1-cm coring on side 2, further extension was observed at nearly all locations on the block, with the exception of slight increases of radial compression around the freshly cut surface. Thus, it seemed that the interior restraints or balances had been partly destroyed or damaged so that the block expanded.

BEHAVIOR OF BLOCK — TOTAL EXPERIMENT

The net strains for the entire experiment on the bottom annuli (fig. 11*B*) are radially compressive and tangentially extensional. On the same surface, the exterior rind has nearly zero radial strains (gages 14, 21, 26) but has large extensional tangential strains. On side 2 (fig 11*C*), the radial strains (with one exception) are compressional, and the tangential strains are all extensional. The two remaining locations (gages 7, 13) on the top surface (fig. 11*A*) In general, the final net strains seem to indicate that the central core, both annuli, and the remaining parts of the block are radially shortened and tangentially expanded. The radial compression decreases outward, whereas the tangential extension increases outward.

BEHAVIOR OF BLOCK — SUMMARY

The foregoing discussion shows that stress relief and the resulting strains manifested at free surfaces of the block are very complex. The residual state of stress within the body changes in a complex manner as new boundaries (free surfaces) are introduced.

The initial strain changes, as the block of granite was cored on the top surface, indicate that the mobilized part of the residual stress field was tensile in sense — that is, all the relieved strains had been compressive. Yet, as more data were gathered from further coring of the block, many gages expanded, implying that certain compressive elements of the residual state were relieved. For example, the data recorded before and after the final 10.1-cm coring on side 2 indicate that a nearly totally compresssional component of the residual stress field was relieved. The net strain changes for the entire experiment, however, were radial compressions and tangential expansions.

Because the force field within the block had to be internally balanced, the question arises as to why all the initial relieved strains had the same sense. One has to inquire: What are the stress-storage and release mechanisms that allow such deformation to occur? According to McClintock and Argon (1966, p. 434), residual stresses occur on a microscopic scale in metals as a result of anisotropic plastic behavior, dislocations, and inclusions; they occur on a macroscopic scale as a result of

plastic flow or creep and volume changes caused by metallurgical or cchemical processes. Jaeger and Cook (1969, p. 362) alluded to viscoelastic effects to account for residual stresses in rocks. Varnes (1969, p. 417) wrote of frictional, time-dependent, and elastic restraints as attributes of internally balanced stress fields. Bjerrum (1967, p. 45) concluded that diagenetic bonds that welded clay particles together while under maximum consolidation load account for locked-in strain energy of clay deposits. Seemingly, from these statements, the storage of elastic strain energy requires a permanent or time-dependent change of rock structure that fixes or locks-in energy imparted by internal or external force fields. The locking elements can be thought of as passive restraints preventing the active elastic energy from escaping. At any point in the rock, however, there must be a balance of forces to maintain static equilibrium. Thus, the passive restraint elements must provide sufficient resistive forces to balance the active forces that result from stored elastic energy. If the passive restraints are destroyed or if they decay with time, the active elastic energy is mobilized, and strains result.

An analogy of this can be seen in Gallagher's (1971, p. 92) model, in which he applied a biaxial compressive load to an aggregate of photoelastic disks and simultaneously cemented the aggregate. Upon removing the external loads, he found reduced compressive elastic strains stored in the disks, locked in or balanced by the cement. In Gallagher's experiment, the cement was elastic and did not allow a viscous relief of the stored energy. However, if the cement were viscous, the stored strain energy contained in the disks would, in time, be totally relieved. Inasmuch as the cemented model was in a compressed state, the strains relieved within the disks by the viscous relaxation of the cement would be extensional. Relieved strains of compressive sense would, however, occur locally as the cement matrix relaxed. From this example it is inferred that the internal forces resulting from the stored energy must be essentially balanced at any particular time becuase there are no externally applied forces; yet, as the cement relaxes with time, the same stored energy will create measurable extensional strains at the boundaries of the model.

In figure 17*A* a schematic approach similar to that presented by Varnes (1969, p. 419) demonstrates how energy release, caused by permanent and elastic deformations, may generate net strains of only one sense. Figure 17*A* shows the initial equilibrium condition of a hypothetical residual stress model after external restraints and (or) loads have been removed. The restraining and pushing elements represent, respectively, interior tensional and compressional forces that must be equal at equilibrium. The separation of units is an arbitrary linear distance between elements of the model. Changes in this distance thus represent strains.

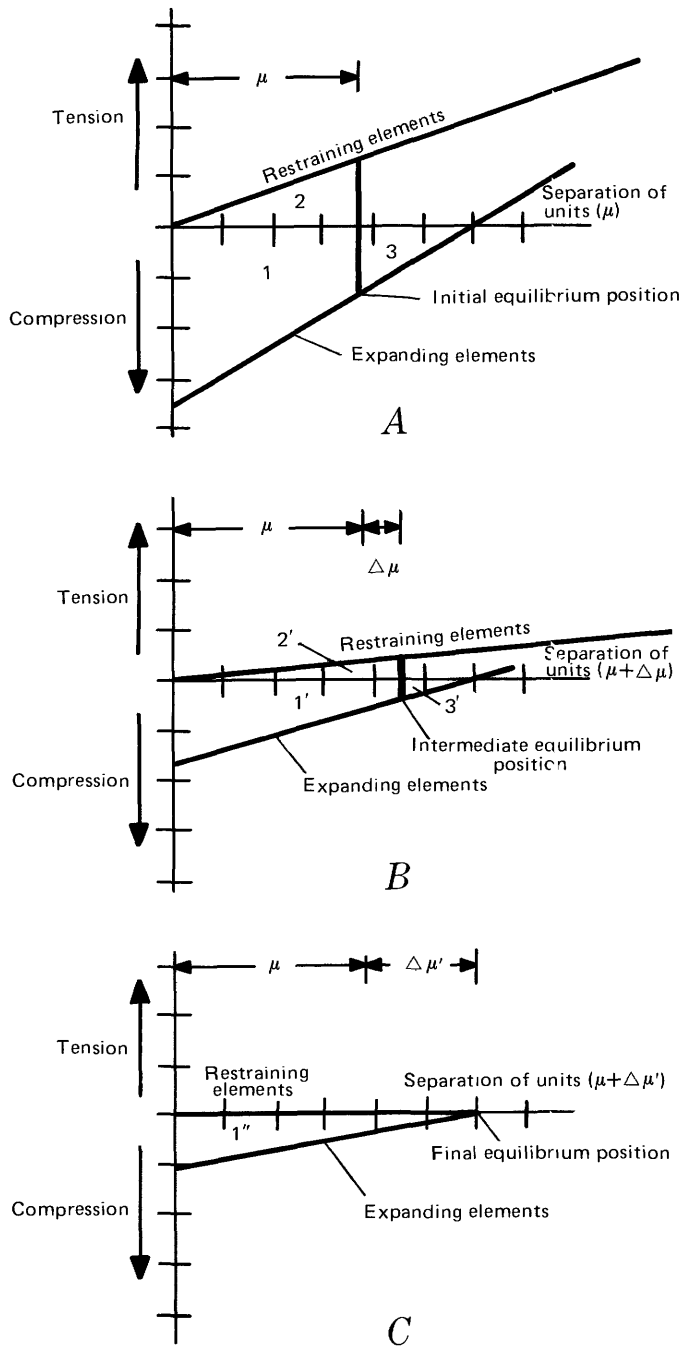

FIGURE 17. — Changes of stored energy in a residual energy model resulting from elastic and permanent deformations of the model elements. Areas 1, 1', and 1'' show work done. Areas 2 and 2' show stored tensile energy in the restraining elements, whereas areas 3 and 3' show stored compressional energy in the pushing elements. *A*, Initial equilibrium condition with external restraints removed. *B*, Partial release of energy after some deformation of restraining elements. *C*, Complete release of energy after deformation of restraining elements.

Area 1 represents the work done in attaining equilibrium, area 2 shows the stored tensile energy, and area 3 shows the stored compressional energy. Figure

17*B* shows the changes that occur when elastic and permanent deformations of the elements are introduced into the model. Assume that the permanent deformations cause a change of modulus for both the restraining (passive) and pushing (active) elements. In the model shown here, the moduli of these elements have been successively softened by decreasing, in equal increments, the angle of slope shown for the elements, thereby allowing the equilibrium position to migrate. The amount of remaining stored energy shown by the areas of triangles 2′ and 3′ has decreased, allowing the units to separate by an amount $\Delta\mu$.

Finally, as shown in figure 17*C*, permanent deformation has completely relaxed the restraining bonds, and no more energy is stored in the system, and a net extensional strain is inferred by the increased separation $\Delta\mu'$ of the units. Therefore, the release of stored energy by means of permanent and elastic deformations is accomplished by extensional strain. Compressional strains on this model are very local, being in the vicinity of the bonds being destroyed by permanent deformation and, thus, are not seen in the illustrated net strain.

The same model may be used for the granite block by inverting the compression and tension axes in figure 17, thereby allowing the release of stored energy by compressional, rather than extensional, strains. The horizontal axis, instead of being "separation of units," becomes "contraction of units." In this model, stored energy when relieved causes compressive strains.

As the block was cored on the bottom and side 2, further relieving the internal stress field, extensional strains became predominant. Up to this time the mobilized component of the residual energy largely produced compressional strains. Thus, the internal stress state seemingly was modified so that extensional strains instead of compressional strains became mobilized. The new internal balance of forces can be explained by the superposition of the unrelieved part of the residual force field and newly freed forces that were generated by mobilized residual strains. These forces, just freed from locally balanced fields, must find new restraints within the body in order to become balanced again. The new restraints are defined by the body material and are modified by the body's geometry. Thus, as the new forces are distributed over the body, each point in the body will have a new equilibrium condition. The geometric controls provided by the new boundaries help in part to determine the nature (direction and magnitude) of the superposed forces, because the boundaries must completely contain these forces. A force field controlled by geometry will generally have uniform gradients of both tension and compression in order to maintain equilibrium. Accordingly, both compressional and tensile strain components can be expected upon relieving the field. In the granite block, possibly such a superposed geometric stress field, created by the initial overcoring, was being relieved as additional coring proceeded; therefore, both tensional and compressional strains were observed.

In all rock types the balanced internal force field at a point is probably some combination of a boundary-induced geometrically controlled force field superposed upon a local intergranular or intragranular force field. Each of these fields, in itself, balanced, but at any point in the rock mass, the combined fields are balanced.

COMPARISON OF RELIEVED STRAINS WITH X-RAY PRESTRESS DETERMINATIONS

The X-ray technique described by Friedman (1967) was used to measure the three-dimensional state of prestress or residual elastic strain in the quartz grains of the granite block. The 19 × 16 × 6 mm chip of granite used for the determination was taken from the top, directly under gage 4, less than 0.1 mm below the surface. If residual strains are locked in the rock, ideally they should be equual in magnitude, but opposite in sign, to the strains obtained by completely removing the restraints.

Because the relieved strains are a function of the geometry of the block and core surfaces and of the changing residual stress as the block was successively cored, the only valid comparison is that of the strain changes at gage 4 in the center of the top surface with the X-ray prestress determined at this location. This prestress, determined by Friedman (in Handin, 1972), is shown by vectors in the lower right part of figures 6 and 7*D*. The principal strain changes at gage 4 are compatible to the X-ray-determined prestress at the same location, in both sense and direction, but have diminished magnitudes.

The following evidence illustrates the point that the residual stresses changed as the geometry of the block and cored surfaces changed. The X-ray-determined prestress in another granite chip of the same master granite block from which the block for this experiment was taken ($\epsilon_1 = 130 \times 10^{-6}$ horizontal and bearing N. 40° W., $\epsilon_2 = -65 \times 10^{-6}$ and vertical, $\epsilon_3 = -250 \times 10^{-6}$ horizontal and bearing N. 50° E.), is very different from the prestress determined at gage 4. The variation of residual stress is further corroborated by the general lack of agreement between the X-ray data at gage 4 and the strain changes that occurred over the rest of the block. Thus, the prestress within the granite may change considerably at any location as a result of changing restraints and body geometry.

The behavior of the block of Barre Granite, however, implies that the small X-ray chip at gage 4 should be greatly relieved as compared with the original block of rock. this is also demonstrated by the fact that the strain changes, induced in shall chips as they are fractured away from an already partly relieved annulus, are very

large (fig. 9*C*), yet, these chips are not as small as those used for X-ray analyses. The relieved strains at gage 4 superposed upon the residual stresses remaining in the cip must represent the original prestress; hence, the relieved strains should be compatible in sense and orientation to the prestress in the chip.

The prestress as measured with X-rays may represent a diminished surface prestress that reflects the principal axes of the residual stress in the larger rock mass, or it may reflect a modification thereof. Moreover, differences can arise between the states of stress measured by X-rays and strain-relief techniques that are attributed to heterogeneous residual strains which, when viewed on the scale of the quartz crystal, give rise to local variations in measurement.

Interestingly, the X-ray-determined prestress directions and relative magnitudes on the chip from the master granite block are in good agreement with the principal axes of the ultrasonic velocity and attentuation determined by Bur, Hjelmstad, and Thill (1969), whereas the X-ray-determined prestress and strain-relief data on the experimental block are not in good agreement with the ultrasonic data.

At this point one wonders how small or how large the stress-locking domain is, if in fact there is more than one locking domain, and if a locking-domain gradient exists. The term "stress-locking domain" as used here has been defined by Varnes and Lee (1972, p. 2865) as "that volume and shape within a particular rock that can contain a balanced force system of a certain maximum intensity without application of exterior loads." Friedman (1968) experimentally demonstrated that residual strains in individual quartz grains within quartzose sandstones relax virtually to zero when etched by hydrofluoric acid, thus implying that the stress-locking domain must be larger than an individual grain. On a much larger scale, one can imagine large locking domains controlled by the original geometry and the geometries of progressive solidification of a granitic pluton. Between these two extremes it is quite probable that there is a locking-domain gradient which may be interrupted by local discontinuities and tectonic structural elements that in themselves define discrete locking domains.

RELIEVED RESIDUAL STRESS FIELD AND COMPARISON WITH IN SITU DETERMINATIONS

RELIEVED RESIDUAL STRESSES

Because the stresses relieved are complexly distributed, there was no attempt made to compute a stress ellipsoid representing the preexisting stress state within the undisturbed block. The behavior of the block adequately demonstrates that the state of residual stress is controlled by the prestress condition and by geometry of the overcores and the block. It is questionable that elastic compliances measured in the laboratory are equal to the in situ compliances because unavoidable permanent structural damage occurs as a result of coring the laboratory samples. However, to get some idea of the magnitudes of these stresses, the principal strain changes shown on the central top core (gage 4) and the outer annulus (gages 2, 6, 9, 12, fig. 8*B*), after the top 15.0-cm coring, and on bottom central core (gage 17) after the bottom 5.1-cm coring (fig. 9*A*), were converted to average principal stress changes (table 4) on the assumption that the rock is elastically isotropic. The same sign convention is used for stress as was used for strain. The stress-change ellipses for the central cores, by changing signs, represent the relieved part of the residual stress field, as presented in table 4.

No attempt is made to correct for the strong elastic anisotropy that has been demonstrated by several investigators (Douglass and Voight, 1969; Hooker and Johnson, 1969; Bur and others, 1969). The Young's modulus (E_t) used to calculate these values is an average of the maximum and minimum tangent moduli determined by Douglass and Voight (1969) on a similar block of Barre Granite from the 40-meter level in the Smith quarry.

RELIEVED RESIDUAL STRESSES COMPARED WITH IN SITU STRESS FIELD

In table 3 it was pointed out that relieved residual stresses can be sizable. To compare the values of the strains and the resulting calculated stresses observed in this experiment with in situ stress measurements, the strains are first reduced to deformations and, thence, to stresses by calculations similar to those of the U.S. Bureau of Mines (Merrill and Peterson, 1961; Hooker and Johnson, 1969). The assumptions used herein for the conversion of strains to deformation are tenuous; nonetheless, despite the lack of corroborating deformation data, they are useful to demonstrate in the following calculations that strains derived from freed residual stresses may be significant components of deformations measured by in situ overcoring techniques.

A standard method for determining the in situ state of stress is analogous to determining the theoretical state of stress in an externally loaded elastic isotropic plate from the measured deformations of a pilot hole within the plate. The method assumes the condition of either plane strain or plane stress and also assumes the rock mass to be elastic, isotropic, and infinite in extent. If the rock mass behaves anisotropically, measurements can be made to account for this anisotropy (Hooker and Johnson, 1969). However, for the purpose of the following calculations, the Barre Granite is here regarded as isotropic.

The method of calculating in situ stresses for a three-axis borehole-deformation gage requires that defor-

TABLE 4. — *Stress changes determined on the top central core and on the outer annulus after top 15.0-cm coring*

Segment	Principal strain changes ($\times 10^{-6}$)		Principal stress changes (bars)		Equivalent relieved residual principal stresses (bars)		Bearing	
	$\Delta_0\epsilon_2$	$\Delta_0\epsilon_1$	$\Delta_0\sigma_2$	$\Delta_0\sigma_1$	$\sigma_2 r$	$\sigma_1 r$	$\sigma_2 r$	$\sigma_1 r$
Outer annulus (average).	−218	39	−76	−6	6	76	Tangential to annulus.	Radial to annulus.
Top central core.	−85	−53	−36	−27	27	36	N. 3° E.	N. 87° W.
Bottom central core.	−85	−35	−30	−22	22	30	N. 78° E.	N. 12° W.

mations be measured across three different diameters of a pilot hole as the stress field around the hole is relieved by concentric overcoring. Thus, any applied forces are removed, and the borehole-deformation meter records the elastic deformation (change in diameter) of the original hole in three directions, generally 120° apart. The borehole-deformation data are used to determine the change in the stress field that occurs upon relief of the applied forces. In that the calculated stress changes are inferred to be equal and opposite to the applied stress field, one merely inverts the sense of the calculated stresses and implies that these data represent the true in situ stress field. This approach works well if the forces acting on the borehole are, in fact, applied at a distance and are not internal (residual).

In the block of Barre Granite, there are no applied boundary forces, and the deformations are generated merely by cutting away parts of the block to relax all or part of the residual stresses. The central borehole is the first to be cut, and, as can be inferred by the radial compression and tangential extension seen in figure 6, the hole expands upon cutting. Then, as the inner and outer annuli are cut, the hole continues to become larger, yet the rock mass is becoming smaller, seemingly as the result of relieving internally stored tensile energy. However, for the central hole to become larger as a result of cutting boundary forces, these forces would have to be compressional. Thus, an identical deformation of the central hole can be obtained from two quite different states of loading — one consisting of external compressive forces, and the other consisting of excess tensional energy stored internally.

Unfortunately, the deformations across the central hole could not be measured during the experiment; therefore, they must be determined on the basis of measured strains surrounding the hole. Also, because the strain-gage rosettes were placed diametrically across the hole in only two orthogonal directions, deformations can be determined only in these directions. The deformation in a third direction was calculated from knowledge of the ratio of in situ stresses, as determined by Hooker and Johnson (1969) in the field.

To determine the diametral deformations of the inner core hole, the inner and outer annuli are considered to be a composite hypothetical annulus, about 5.1 cm thick, to approximate the geometry of an in situ stress determination. The strains of the two annuli are reasonably uniform in magnitude and direction, and, thus, they are superposed by averaging along the same radial direction. The strains so determined are assumed to be the average values of the single 5.1-cm annulus.

From the strains recorded as the 5.1-cm borehole was initially cut, it can be seen that there was significant deformation adjacent to the borehole and outward to within 25.4 mm of the wall. Further strains that occurred by making the 15.0-cm drill cut then relieved the rest of the annulus. The radial strains were all compressive, and calculated deformations indicate that the borehole wall moved out. The median circumferences of both annuli, comprising the hypothetical annulus, were displaced with respect to their initial positions occupied before the 5.1-cm overcoring. As illustrated in figure 18, the median circumference of the inner annulus was determined by circular deformation to be displaced inwardly 91×10^{-6} cm, and the median diameter of the outer annulus was displaced outwardly 245×10^{-6} cm. If the relative displacements of both annuli are taken into account, a summed neutral circumference of zero radial deformation for the composite hypothetical annulus can be located outward at slightly greater than three-fourths of the way between the inner and outer surfaces of the outer annulus. This is 5.5 mm from the outer surface, or 45.3 mm from the inner borehole boundary. If the strains $\Delta_0\epsilon$ are assumed to be nearly uniform in the radial direction, the inner radial borehole deformation (U_R) in any direction on the annulus created by a 15.0-cm core bit, can be calculated from the neutral circumference by summing the average strains over the estimated distances of deformation, $U_R = 45.3 \times$ "ϵ_R annulus" − (25.4 "ϵ_R borehole + 72"), where "ϵ_R annulus" is the average radial strain of the annulus "ϵ_R borehole" is the average radial strain adjacent to the borehole, and the $+ 72 \times 10^{-6}$ is the average radial circular deformation that occurred prior to cutting the outer annulus. The diametral deformation is expressed as $U_d = 2\ U_R$. The following diametral deformations U_1, oriented N. 30° E., and U_3, oriented 90° to U_1, were calculated for the top surface.

$U_1 = 1{,}142 \times 10^{-6}$ cm and $U_3 = 1{,}710 \times 10^{-6}$ cm, extensional deformations.

Using equations for the 45° rosettes (Merrill and Peterson, 1961), and using the ratio of the in situ principal stresses already determined by Hooker and Johnson (1969) at the Smith quarry, one can approximate values of stress relief in the granite.

$$S + T = \frac{E}{2d} \quad (U_1 + U_3),$$

$$U = \frac{d}{E} [(S + T) + 2 (S - T) \cos 2\theta],$$

where

S and T = major and minor secondary in situ principal stresses, respectively;
d = diameter of borehole = 5.1 cm;
E = Young's modulus = 3.41×10^5 bars; and
θ = counterclockwise angle from S to U.

Thus, $S + T = -95$ bars.

Hooker and Johnson's data (1969) show that the ratio S/T is 0.51 for the state of stress (isotropic assumption) at the 100-m level in the Smith quarry. Assuming that this ratio is nearly the same for my block taken at the 67-m level of the Wetmore and Morris quarry, $S = 0.51T$, and $T + 0.51T = -95$ bars; and in figure 19 the in situ stress or inferred exterior load is then:

$T = -63$ bars Bearing of T = N. 6° W.
$S = -32$ bars Bearing of S = N. 84° E.

The "isotropic" values of S and T determined by Hooker and Johnson (1969) at the surface (1) and at the 100-m level (2) are

(1) $T = -32$ bars $S = -8$ bars Bearing of T = N. 27° E.
(2) $T = -188$ bars $S = -96$ bars Bearing of T = N. 14° W.

By comparing all these values one can readily see that the estimated deformations caused by relieving residual stresses may be significant components of the total measured in situ deformations. Further, as demonstrated here, the residual stress orientations and magnitudes are similar enough to the in situ determinations that the in situ stress field could be entirely residual.

DEFORMATION MECHANISMS

It has been suggested that fractures are produced upon relieving crystalline rocks from high in situ stress concentrations (Hooker and Duvall, 1966, p. 14). The permanent structural damage caused by such opening of fractures, according to Norman (1970, p. 21), can occur within cores as they are removed from the outcrop. Norman demonstrated that the microfractures in crystalline rocks near Atlanta, Ga., are preferentially oriented normal to the axis of maximum strain relief, and he attributed much of the nonlinear deformation in this direction to the opening of fractures.

FIGURE 18. — Exaggerated illustration of deformations, following the top 15.0-cm coring, of the inner and outer annuli. The deformations are relative to the initial annuli positions prior to the 5.1-cm coring. Solid lines show the initial positions; dashed lines show the final positions. Distances between dashed and solid lines represent deformations. ▷

However, the block of Barre Granite, as it was being relieved by coring, showed very little evidence of new fracturing. During the initial corings the minor principal strain changes were all radially compressive, and the magnitudes appeared to change uniformly away from the cut. It is difficult to imagine fractures opening in such a strain field. If fracture development were a dominant mechanism, one would expect a very erratic behavior under the strain gages wherever fractures occurred. No such behavior was observed until the strain changes started to become extensional. Figure 8*C* and *F* and 9*A*, *B*, and *E* show anomalous strain changes that developed at one location (gage 22) as extensional strain changes become more dominant. Figure 9*C* shows strain changes at gage locations on the interior annulus that have obviously been freed by bounding fractures (fig.4). These changes are very large, and they appear to be somewhat random in orientation, which implies localized stress changes that are probably caused by fracture development or grain-boundary movement.

The photographs of dyed areas before and after drilling (fig. 14) show little or no evidence of new fracture development except immediately adjacent to the newly cut surface. Figures 14*A* and *B* show a location on the outer annulus at which some of the largest strains occurred. Even though existing microfractures are plainly visible, a comparison of the before and after photographs shows no new fracturing except within 2 mm from the new surface. Similarly, the photographs of a location nearer the edge of the block that experienced much less strain show no new microfractures (figs. 14*C*, *D*).

The general lack of fracture development upon stress relief is consistent with the conclusion of Nur and Simmons (1970) that microfractures are not introduced during drilling unless the stress field is very high. It is suggested, therefore, that the deformations observed in the Barre Granite black were largely elastic. The permanent structural damage, of the kind alluded to by Norman (1970), probably occurred in lesser amounts and most likely was accomplished by slip along grain boundaries or possibly even by intragranular-creep mechanisms.

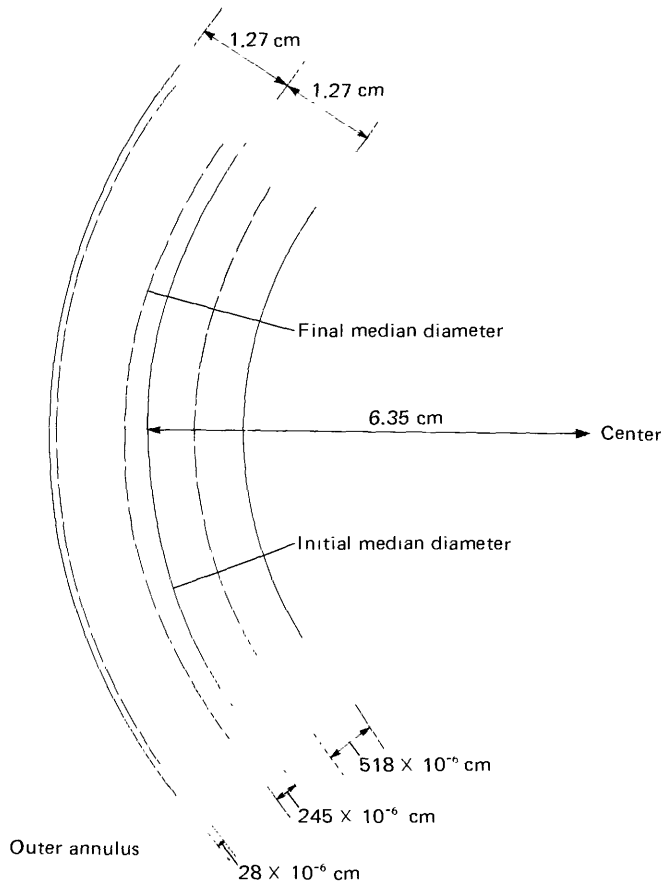

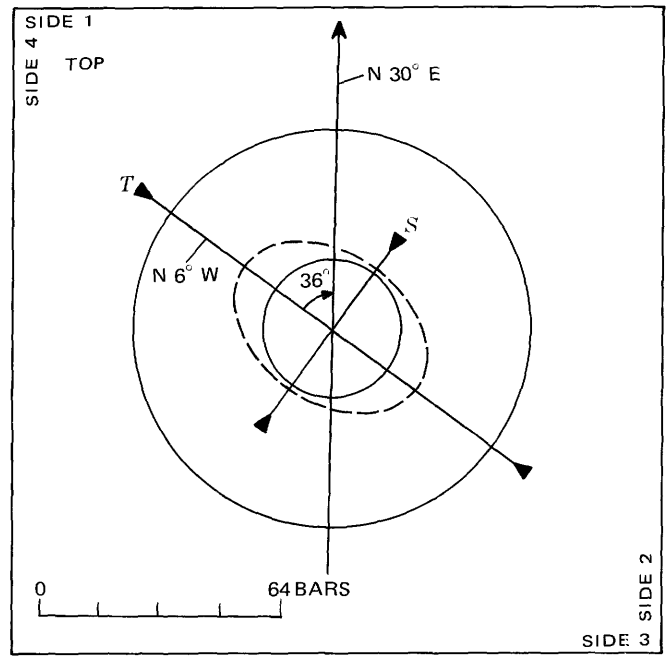

FIGURE 19. — Inferred in situ stress vector components calculated from deformations of the block of Barre Granite. S is maximum principal stress (least compressive). T is minimum principal stress (most compressive). Dashed line shows exaggerated deformation ellipse.

RELATION OF FABRIC ANISOTROPY TO RESIDUAL STRESS FIELDS

There are strong preferred orientations of fabric elements in the Barre Granite that have been determined by previous investigators. Douglass and Voight (1969) have found microfractures and fluid inclusions to be strongly oriented parallel to the rift direction or the plane of easiest parting, which in the Barre Granite is vertical and strikes about N. 30° E. They have found a small concentration of microfractures parallel to the horizontal grain or lift. According to Douglass and Voight, microfractures and fluid inclusions are the fabric elements most influential to the mechanical behavior of the granite. Directions normal to microfractures and fluid-inclusion planes are parallel to the direction of maximum compliance and the direction of minimum tensile strength. In addition, the quartz optic axes are strongly oriented nearly parallel to the rift plane.

Willard and McWilliams (1969) found a similar strong concentration of microfractures parallel to the plane of easiest tensile fracture (the rift plane).

Other manifestations of the anisotropy are the measured sound velocities and relative amplitudes within the Barre Granite (Bur and others, 1969), which show well-developed orthotropic symmetry. The plane defined by the maximum and intermediate axes of the velocity and relative amplitude fields nearly coincide with the rift plane (M. Friedman, oral commun., 1971).

Cursory examinations of three mutually perpendicular thin sections taken from my block reveal that the densest microfracture sets are parallel to the rift and lift plane (fig. 15). There, the fractures in the lift plane are apparently better developed than those in the rift plane. These results do not agree with those of Douglass and Voight (1969), who found the fracturing in the rift plane and the least in the plane of lift. Thus, either there are local variations of fracture spacings or one must entertain the possibility that the block is misoriented. In that the orientations have been rechecked and found to be correct, it is assumed that there are localized variations in the fracture development.

Although the fabric elements definitely are related to deformational behaviors observed in the laboratory and in quarry operations, a similar relation to either the in situ stress field or the residual stress field is not as clear. The average bearings for the minimum and maximum principal stresses determined in situ by Hooker and Johnson (1969) are, respectively, N. 14° E. and S. 76° E. However, at the two sites they tested, the orientations corrected for anisotropy are variable; for example, σ_2 ranges from N. 8° W. to N. 32° E. The inferred minimum principal stress determined by the method of Hooker and Johnson on my block, corrected for anisotropy, has a bearing of approximately N. 1° W. The minimum principal relieved residual stresses as determined by calculation of a stress ellipse on the top and bottom central cores (table 3) have bearings of N. 3° E. and N. 78° E., respectively. Therefore, stresses calculated by relieving the in situ stress field and (or) the residual stress field do not seem to relate very well to the velocity or fabric data, which coincide with the rift-plane strike of N. 30° E., or to the hardway plane (plane of maximum tensile strength). The perpendicular alinement of most microfractures to the minimum principal stress, as observed by Norman (1970) in the Georgia rocks, does not hold here, so it does not seem reasonable that stress-relief microfracturing appreciably influences the measurement of residual stresses.

In that no fabric elements seem to aline with the principal directions of stress relief, it is difficult to relate residual stresses to any strong fabric anisotropy. The reasons for this lack of correlation are not at all clear from this study, but there are some indications. Some of the fabric elements seen during microscopic examination suggest possible mechanisms of locking stresses in. The granite has clearly undergone deformation sometime during its history. The quartz grains show large amounts of undulatory extinction, and the feldspar and quartz grains are highly fractured. Also, the presence of small grains that have formed along larger feldspar- and quartz-grain boundaries is evidence of syntectonic recrystallization.

Dislocation motions probably occurred within the constituent minerals, as indicated at least for quartz by the undulatory extinction, to produce self locally balanced stress fields. After the geologic deformation attenuated, the rock fabric contained large amounts of elastic strain energy locked in or keyed in by dislocations, grain-boundary restraints, and external restraints on the rock mass as a whole. The cutting of new surfaces removed the external restraint and caused permanent deformations, such as new fractures, grain-boundary slip, and renewed dislocation activity that allowed the relief of local restraints. Deformation then continued until the internal forces again became balanced by the restraints. McClintock and Argon (1966, p. 420) said that, in metals, "residual stresses arise from dislocation pile ups, kink boundaries, deformation-induced tilt boundaries, deformation twins and other diffusionless shear transformations." In such a manner, anisotropic elastic or viscoelastic strain energy could be stored within a rock mass without any apparent relationship to fabric anisotropy.

Carter (1969) calculated the stress required for specific edge-dislocation spacings genetically associated with quartz deformation lamellae. A spacing of 315 angstrom units, or 3×10^5 edge dislocations per centimeter, can account for the observed change of birefringence across the lamellae of 0.002. The differential stress necessary for a stress-optical effect of this magnitude is about 5.4×10^3 bars ($\sigma_{11} \times 10^3$ bars and $\sigma_{22} = 0.8 \times 10^3$ bars). Thus, owing to permanent deformation, large stress differences can be stored within the grains of the rock. The stored stress associated with the deformation lamellae can be relieved if the dislocations migrate such as to reduce their density along the lamellae. It is not known whether the dislocations move at room temperature upon relaxation of constraints about a given grain. Clearly, lamellae do exist in freed, isolated quartz grains.

In the Barre Granite the relieved stresses are 1 or 2 orders of magnitude less than the values calculated by Carter (1969). However, deformation lamellae are not conspicuous in the granite, and the only evidence of dislocation lineups is the undulatory extinction. Nonetheless, sufficient locked-in energy can probably be associated with dislocations alone to account for the residual stress in the Barre Granite, provided that even a fraction of that energy is recovered.

The actual mechanisms of storing residual stresses cannot be determined from microscopic petrofabric studies, simply because the specimens become relieved when they are prepared for observation. With existing techniques it is impossible to look at the "before" (natural) state.

In light of Carter's (1969) calculations, however, an indirect approach for estimating residual stresses can be

used; for example, the approach can be used to statistically compare the relative development of intensity of deformation lamellae or undulatory extinction to the magnitude of relieved residual stresses.

SPECULATION AND POSSIBLE FUTURE WORK

The relieved strains measured in this experiment indicate that there are large amounts of potential strain energy stored in rock masses which are capable of being mobilized when new surfaces are created. To know the geometry and size of these stored-energy regimes and what the mechanisms are that store and relieve them would be of great practical value. The mobilized energy alluded to undoubtedly contributes to the deformational behavior of rock masses in mining and quarrying operations, as well as in dam excavations. Significant quantities of energy stored as residual strain conceivably may be relieved in large-scale fracturing of rock masses, as in earthquakes. Therefore, the relieved energy may contribute to overall behavior of earthquake events, especially the aftershocks.

As has already been suggested by others (Varnes, 1969; Durrance, 1969), the release of strain energy is probably a significant factor in mechanical-weathering processes. Certainly, the relieved strains measured in this experiment would indicate that relieved strains can either aid or hinder mechanical-weathering processes. For example, if the residual-energy state is such that the resulting relieved strains are extensional, the mechanical weathering would be abetted; whereas, if the residual-energy state is such that the relieved strains are compressive, the mechanical weathering would be hindered.

Future work attempting to define the mechanisms that store residual stress in rocks and to determine how these same mechanisms relieve stress will be important. Determining how large the stress-locking regimes can be and how much available energy may be present within any regime are also important. A definition of the geometry of these regimes may give clues as to the genesis of the residual stress.

CONCLUSIONS

The conclusions to be drawn from the release of residual stresses by drilling concentric slots of successively larger diameter in a block of Barre Granite are as follows:

1. The relieved strains are large, but because of the changes with successive cuts, the strains are not compatible with the calculation of a unique residual-stress tensor for the block. These strains show that significant quantities of stored strain energy can be mobilized.

   After the top of the block had been cored, the relieved compressive strains indicated that initially there was an excess of tensile residual energy in the block with a relieved tensile maximum-principal-stress component of at least 6 bars.

   As the coring was continued on the bottom and on side 2, the relieved strains became more extensional, indicating that the residual stress had become more compressional.

   Finally, the net strains indicated that the relieved part of the residual stress field was both tensile and compressional, with the minimum principal (compressive) stress being circumferential.
2. Contractions of cores and annuli cannot be caused by the opening of fractures; thus, the deformations produced by stress relief are not accompanied by appreciable new microfracturing.
3. The strains resulting from stress relief are not limited to short distances from the fresh cuts; rather, away from the cuts they diminish uniformly over the entire surface in a pattern related to the geometry of the cuts and the initial shape of the block. The largest strains are adjacent to the new surfaces.
4. Identical deformations measured across a borehole, as a result of stress-relief overcoring techniques, can be produced by two different balanced-stress systems. Mobilization of tensile residual stress energy can produce the same deformation as externally applied compressional forces.
5. Although the anisotropic deformations of the rock are definitely related to the fabric anisotropy, the residual stress is not clearly related to these fabric elements. In fact, the internally balanced stress field seems to change as the geometry of the body changes, yet it maintains an inherent orientation, as can be seen by the elliptical deformation of the annuli. The measured residual stress field is related at least to the geometry of the body and to the degree of homogeniety, orientations, and magnitudes of the originally frozen-in stresses.
6. The X-ray determined prestress was compatible in sense and direction with the strain changes at the same location (gage 4). The magnitudes of the strain changes, however, were smaller than those of the X-ray-determined prestress. Elsewhere on the block, the strain changes were compatible at some locations with only the direction of the X-ray-determined prestress at gage 4.

   The X-ray prestress that is determined in a small chip may represent the direction and sense of the prestress at the same point in the block prior to the dissection of the chip. However, the magnitudes will have been diminished by at least the magnitudes of the relieved strains.

REFERENCES CITED

Bjerrum, Laurits, 1967, Progressive failure in slopes of overconsolidated plastic clay and clay shale: Am. Soc. Civil Engineers Proc., v. 93, paper 5456, Jour. Soil Mechanics and Found. Div., v. 93, no. SM5, pt. 1, p. 1-49.

Bur, T. R., Hjelmstad, K. E., and Thill, R. E., 1969, An ultrasonic method for determining the attenuation symmetry of materials: U.S Bur. Mines Rept. Inv. 7335, 8 p.

Carter, N. L., 1969, Flow of rock-forming crystals and aggregates, *in* Riecker, R. E., ed., Rock mechanics seminar, v. 2: Bedford, Mass., Air Force Cambridge Research Lab., p. 509-594.

Chayes, Felix, 1952, The finer-grained calcalkaline granites of New England: Jour. Geology, v. 60, no. 3, p. 207-254.

Denkhaus, H., 1967, Report on theme 4, residual stresses in rock masses: Internat. Soc. Rock Mechanics Cong., 1st, Lisbon, Portugal, Proc., v. 3, p. 312-319.

Douglass, P. M., and Voight, Barry, 1969, Anisotropy of granites — A reflection of microscopic fabric: Geotechnique, v. 19, no. 3, p. 376-398.

Durrance, E. M., 1969, Release of strain energy as a mechanism for the mechanical weathering of granular rock material: Geol. Mag., v. 106, no. 5, p. 496-497.

Emery, C. L., 1964, Strain energy in rocks, *in* State of stress in the earth's crust — Internat. Conf., Santa Monica, Calif., 1963, Proc.: New York, Am. Elsevier Publishingg Co., p. 234-279.

_____1968, Strain in rocks, *in* Engineering geology and soils engineering symposium, 6th Ann., Boise, Idaho, 1968, Proc.: Boise, Idaho Dept. Highways, p. 355-364.

Friedman, M., 1967, Measurement of the state of residual elastic strain in quartzose rocks by means of X-ray diffractometry: Norelco Reporter, v. 14, no. 1, p. 7-9.

_____1968, X-ray analysis of residual elastic strain in quartzose rocks, *in* Gray, K. E., Basic and applied rock mechanics: Baltimore, Port City Press, Inc., p. 573-597.

_____1971, Residual elastic strains in rock, *in* Studies in rock fracture: U.S. Army Corps Engineers Tech. Rept. 5, Contract DACA 73-68-C-0004, 55 p.

_____1972, Residual elastic strains in rocks: Tectonophysics, v. 15, no. 4, p. 297-330.

Friedman, M., and Logan, J. M., 1970, The influence of residual elastic strain on the orientations of experimental fractures in three quartzose sandstones: Jour. Geophys. Research, v. 75, no. 2, p. 387-405.

Frocht, M. M., 1941, Photoelasticity, v. 1: New York, John Wiley & Sons, Inc., 411 p.

Gallagher, J. J., Jr., 1971, Photomechanical model studies relating to fracture and residual elastic strain in granular aggregates, *in* Studies in rock fracture: U.S. Army Corps Engineers Tech. Rept. 3, Contract DACA 73-68-C-0004, 127 p.

Gardner, R. D., and Pincus, H. J., 1968, Fluorescent dye penetrants applied to rock fractures: Internat. Jour. Rock Mechanics and Mining Sci., v. 5, no. 2, p. 155-158.

Handin, John, 1972, Studies in rock fracture, Task 1: U.S. Army Corps Engineers Quart. Tech. Rept. 17, Contract DACA 73-68-C-0004, p. 2-5.

Hooker, V. E., and Duvall, W. I., 1966, Stress in rock outcrops near Atlanta, Georgia: U.S. Bur. Mines Rept. Inv. 6860, 18 p.

Hooker, V. E., and Johnson, C. F., 1969, Near-surface horizontal stresses, including the effects of rock anisotropy: U.S. Bur. Mines Rept. Inv. 7224, 29 p.

Hoskins, E. R., and Daniels, P. A., 1970, Measurements of residual strain in rocks: Am. Geophys. Union Trans., v. 51, no. 11, p. 826.

Jaeger, J. C., and Cook, N. G. W., 1969, Fundamentals of rock mechanics: London, Methuen & Co., Ltd., 513 p.

Lowry, W. D., 1959, Expansion domes and shear cones in Mount Airy granite [N.C.]: Mineral Industries Jour., v. 6, no. 4, p. 1-6.

McClintock, F. A., and Argon, A. W., 1966, Mechanical behavior of materials: Reading, Mass., Addison Wesley Publishing Co., 770 p.

Merrill, R. H., and Peterson, J. R., 1961, Deformation of a borehole in rock: U.S. Bur. Mines Rept. Inv. 5881, 32 p.

Nichols, T. C., Jr., Lee, F. T., and Abel, J. F., Jr., 1969, Some influence of geology and mining upon the three-dimensional stress field in a metamorphic rock mass: Assoc. Eng. Geologists Bull., v. 6, no. 2, p. 131-143.

Norman, C. E., 1970, Geometric relationships between geologic structure and ground stresses near Atlanta, Georgia: U.S. Bur. Mines Rept. Inv. 7365, 24 p.

Nur, Amos, 1971, Effects of stress on velocity anisotropy in rocks with cracks: Jour. Geophys. Research, v. 76, no. 8, p. 2022-2034.

Nur, Amos, and Simmons, Gene, 1969, Stress-induced velocity anisotropy in rock — An experimental study: Jour. Geophys. Research, v. 74, no. 27, p. 6667-6674.

_____1970, The origin of small cracks in igneous rocks: Internat. Jour. Rock Mechanics and Mining Sci., v. 7, no. 3, p. 307-314.

Pincus, H. J., 1964, Discussion of "Strain energy in rocks," by C. L. Emery (1964), *in* State of stress in the Earth's crust — Internat. Conf., Santa Monica, Calif., 1963, Proc.: New York, Am. Elsevier Publishing Co., p. 269-279.

Price, N. J., 1969, Laws of rock behavior in the earth's crust, *in* Somerton, W. H., Rock mechanics theory and practice: Baltimore, Port City Press, Inc., p. 3-23.

Sharp, J. E., 1969, Engineering geology studies of the Henderson no. 1 shaft, Henderson mine, Climax Molybdenum Co., Empire, Colorado: Denver, Colo., Adm. rept. to Climax Molybdenum Co., 63 p.

Varnes, D. J., 1969, Model for simulation of residual stress in rock, *in* Somerton, W. H., Rock mechanics theory and practice: Baltimore, Port City Press, Inc., p. 415-426.

Varnes, D. J., and Lee, F. T., 1972, Hypothesis of mobilization of residual stress in rock: Geol. Soc. America Bull., v. 83, no. 9, p. 2863-2866.

Voight, Barry, 1967, Interpretation of in situ stress measurements: Internat. Soc. Rock Mechanics Cong., 1st, Lisbon, Portugal, 1966, Proc., v. 3, p. 332-348.

White, W. S., 1946, Rock-bursts in the granite quarries at Barre, Vermont: U.S. Geol. Survey Circ. 13, 15 p.

Willard, R. J., and McWilliams, J. R., 1969, Microstructural techniques in the study of physical properties of rock: Internat. Jour. Rock Mechanics and Mining Sci., v. 6, no. 1, p. 1-12.

☆ U.S. GOVERNMENT PRINTING OFFICE: 1975—677-308/30